

This is the Accepted Manuscript version of an article accepted for publication in Reports on Progress in Physics. IOP Publishing Ltd is not responsible for any errors or omissions in this version of the manuscript or any version derived from it. The Version of Record is available online at <https://doi.org/10.1088/1361-6633/ac8e82>.

Uthe, Brian, John E Sader and Matthew Pelton. "Optical measurement of the picosecond fluid mechanics in simple liquids generated by vibrating nanoparticles: A review." Reports on Progress in Physics 85, no. 10 (17 October 2022). <https://doi.org/10.1088/1361-6633/ac8e82>.

<https://doi.org/10.1088/1361-6633/ac8e82>

Access to this work was provided by the University of Maryland, Baltimore County (UMBC) ScholarWorks@UMBC digital repository on the Maryland Shared Open Access (MD-SOAR) platform.

Please provide feedback

Please support the ScholarWorks@UMBC repository by emailing scholarworks-group@umbc.edu and telling us what having access to this work means to you and why it's important to you. Thank you.

Optical measurement of the picosecond fluid mechanics in simple liquids generated by vibrating nanoparticles: A review

Brian Uthe,¹ John E. Sader,² and Matthew Pelton¹

¹Department of Physics, UMBC (University of Maryland, Baltimore County), Baltimore, MD 21250, U.S.A.

²School of Mathematics and Statistics, The University of Melbourne, Victoria 3010, Australia

Abstract

Standard continuum assumptions commonly used to describe the fluid mechanics of simple liquids have the potential to break down when considering flows at the nanometer scale. Two common assumptions for simple molecular liquids are that (1) they exhibit a Newtonian response, where the viscosity uniquely specifies the linear relationship between the stress and strain rate, and (2) the liquid moves in tandem with the solid at any solid-liquid interface, known as the no-slip condition. However, even simple molecular liquids can exhibit a non-Newtonian, viscoelastic response at the picosecond time scales that are characteristic of the motion of many nanoscale objects; this viscoelasticity arises because these time scales can be comparable to those of molecular relaxation in the liquid. In addition, even liquids that wet solid surfaces can exhibit nanometer-scale slip at those surfaces. It has recently become possible to interrogate the viscoelastic response of simple liquids and associated nanoscale slip using optical measurements of the mechanical vibrations of metal nanoparticles. Plasmon resonances in metal nanoparticles provide strong optical signals that can be accessed by several spectroscopies, most notably ultrafast transient-absorption spectroscopy. These spectroscopies have been used to measure the frequency and damping rate of acoustic oscillations in the nanoparticles, providing quantitative information about mechanical coupling and exchange of mechanical energy between the solid particle and its surrounding liquid. This information, in turn, has been used to elucidate the rheology of viscoelastic simple liquids at the nanoscale in terms of their constitutive relations, taking into account separate viscoelastic responses for both shear and compressible flows. The nanoparticle vibrations have also been used to provide quantitative measurements of slip lengths on the single-nanometer scale. Viscoelasticity has been shown to amplify nanoscale slip, illustrating the interplay between different aspects of the unconventional fluid dynamics of simple liquids at nanometer length scales and picosecond time scales.

I. Introduction: Fluid mechanics at nanometer length scales and picosecond time scales

The study of fluid mechanics dates to at least the time of Archimedes yet remains a highly active field of research, due to its ubiquitous importance in modern technologies, medicine, and engineering. While the modern theory for fluid motion, the Navier-Stokes equation, is relatively simple in mathematical form, it yields tremendous dynamic complexity. Moreover, this theory applies only to the simplest fluids, with a wealth of generalizations possible, depending on the nature of the fluid and on the length and time scales of interest. In particular, when considering liquid flow on nanometer length scales and ultrafast time scales, the underlying assumptions of the Navier-Stokes equation, which are common at macroscopic length scales, may need to be revisited.

Despite additional complications that can arise in liquid motion at nanometer scales relative to their macroscopic counterparts, there is one key approximation that can be made. Much of the complexity of fluid mechanics arises from the inherent nonlinearity of its equation of motion [1]. For liquid flow in or around nanoscale objects, the effects of convective inertia can be generally ignored, rendering the Navier-Stokes equations linear. The importance of convective inertia is quantified by the Reynolds number,

$$\text{Re} = \frac{\rho UL}{\mu}, \quad (1)$$

which defines the ratio of inertial to viscous forces, where ρ is the density of the fluid, U is the velocity scale of the fluid flow, L is the length scale of the flow, and μ is the shear viscosity of the fluid. For micro- and nano-scale flow of liquids, the Reynolds number is generally very small, i.e., $\text{Re} \ll 1$. In this regime and for any liquid, the mass and momentum conservation equations and the equation of state can be linearized [2]:

$$\frac{\partial(\kappa p)}{\partial t} + \nabla \cdot \mathbf{v} = 0, \quad \rho_0 \frac{\partial \mathbf{v}}{\partial t} = \nabla \cdot \mathbf{T}, \quad (2)$$

where p is the pressure, \mathbf{v} is the liquid velocity field, ρ_0 is the liquid density at equilibrium, κ is the liquid compressibility, and \mathbf{T} is the Cauchy stress tensor. The Cauchy stress tensor can in turn be separated into an isotropic (pressure) contribution, $-p\mathbf{I}$, where \mathbf{I} is the identity tensor, and a

contribution that deviates from isotropy, known as the deviatoric stress tensor, \mathbf{S} ; i.e., $\mathbf{T} = -p\mathbf{I} + \mathbf{S}$.

These conservation equations, Eq. (2), require a closure that specifies the manner in which the liquid deforms, i.e., a constitutive equation defining the stress / strain-rate relation. The most common approach is to specify a linear relationship via Newton's law of viscosity; see Figure 1. The generalization of Newton's law of viscosity to any flow is [1]

$$\mathbf{S} = 2 \mu \mathbf{D}, \quad (3)$$

where the rate-of-strain tensor, $\mathbf{D} = (\nabla \mathbf{v} + (\nabla \mathbf{v})^T)/2$, a relation that holds for incompressible Newtonian flows. Substituting these expressions into Eq. (2) recovers the linearized Navier-Stokes equations for Newtonian fluid mechanics, which is commonly used to characterize microscale flows.

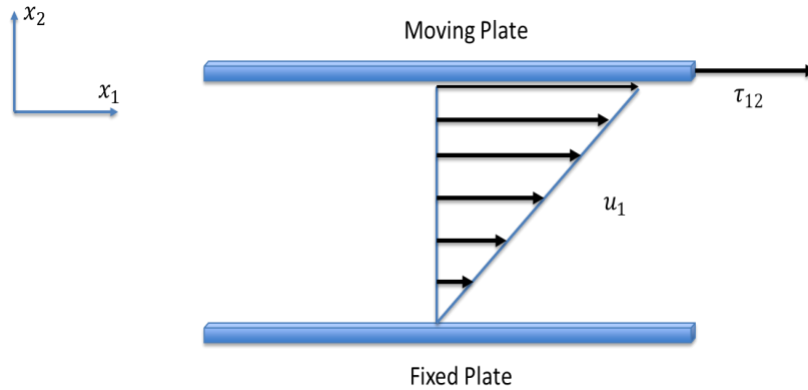


Figure 1. Newton's law of viscosity. For the applied shearing motion, a linear relationship is exhibited between the stress experienced by the plate and the plate's velocity; the coefficient of linearity is the fluid's shear viscosity, μ . The fluid velocity between the parallel plates varies linearly with distance.

Applicability of the Newtonian approximation under time-dependent (unsteady) flow is quantified by the Deborah number,

$$\text{De} = \frac{\lambda}{\tau}, \quad (4)$$

where τ is the characteristic time of the fluid flow and λ is the relaxation time scale for the liquid to return to its equilibrium state after being disturbed. For simple molecular liquids, such as water and glycerol, λ corresponds to the molecular relaxation time for self-diffusion. Fluids can be described as Newtonian when $De \ll 1$, with the opposite limit, $De \gg 1$, corresponding to solid-like, or elastic, behavior. Between these two limits, fluids in general exhibit a complex viscoelastic response [3].

Maxwell's constitutive model for incompressible viscoelasticity specifies the Hookean (solid-like) response of the fluid at high De , together with the Newtonian (fluid-like) behavior at low De , in a single equation [4]:

$$\mathbf{S} + \lambda \frac{\partial \mathbf{S}}{\partial t} = 2\mu \mathbf{D}. \quad (5)$$

This Maxwell model recovers Newtonian behavior for $De \ll 1$ and is modeled mechanically by a spring and dashpot in series (see Figure 2a). The complementary parallel arrangement produces the Kelvin-Voigt model, exhibiting solid-like behavior in the same (slow deformation) regime. The Maxwell model can be generalized to incorporate greater complexity, including a spectrum of relaxation times.

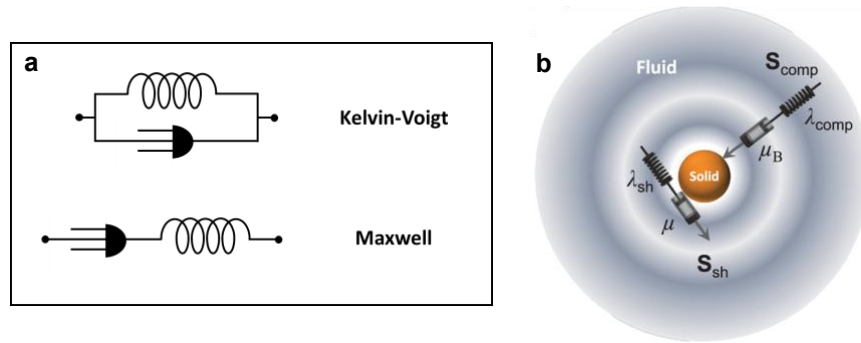


Figure 2. (a) Schematics for linear viscoelastic models. The Kelvin-Voigt model has a spring and dashpot in parallel, while the Maxwell model has the spring and dashpot in series. (b) Schematic of the viscoelastic shear and compressional liquid stress acting on a vibrating solid spherical particle. The vibrating sphere

produces outgoing compression waves in the liquid. The shear and compressional stresses act independently of one another. From Ref. [5].

Viscoelasticity is commonly associated with “complex” fluids that have long relaxation times on the order of seconds; examples include colloidal suspensions, emulsions, and polymeric melts [6,7]. However, even simple liquids, consisting of a homogeneous distribution of molecules, can exhibit viscoelastic behavior due to self-diffusion of their constituent molecules; i.e., an elastic response is expected for flows occurring on the time scale for molecular rearrangement. For simple molecular liquids such as water and glycerol, this time scale is at the picosecond level. This ultrafast time scale is also characteristic of the motion of vibrating nanoscale solid objects, meaning these objects should naturally generate viscoelastic flows when immersed in simple molecular liquids.

Several generalizations of the Maxwell model have been proposed for compressible viscoelastic flows, with one that recovers the required fluid and solid behavior in their respective low and high Deborah limits being [5,7]

$$\mathbf{S}_{\text{sh}} + \lambda_{\text{sh}} \frac{\partial \mathbf{S}_{\text{sh}}}{\partial t} = 2\mu \left(\mathbf{D} - \frac{\text{tr} \mathbf{D}}{3} \mathbf{I} \right), \quad \mathbf{S}_{\text{comp}} + \lambda_{\text{comp}} \frac{\partial \mathbf{S}_{\text{comp}}}{\partial t} = \mu_{\text{B}} (\text{tr} \mathbf{D}) \mathbf{I}, \quad (6)$$

where λ_{sh} and λ_{comp} are the shear and compressional relaxation times, respectively, and the deviatoric stress tensor is $\mathbf{S} = \mathbf{S}_{\text{sh}} + \mathbf{S}_{\text{comp}}$, where μ_{B} is the fluid’s bulk (compressional) viscosity.

The conservation equations, Eq. (2), and constitutive equation, Eq. (6), provide a complete theory that can describe the flow of a compressible, linear viscoelastic liquid in the low-Reynolds-number (linear) limit. We note that these equations, like the more conventional Navier-Stokes equation, are based on approximating the liquid as a continuum. This approximation breaks down when the separation between the molecules is comparable to or larger than the length scales of interest. For example, nanoscale flow of gases cannot be described using the continuum equation, necessitating the use of alternative descriptions such as the Boltzmann transport equation. For simple liquids, by contrast, the continuum approximation can continue to be applied even down to the nanometer scale.

To describe the interaction between a flowing liquid and a solid structure, boundary conditions are required at the solid-liquid interface. The normal component of the fluid velocity must match that of the solid at their interface; this is known as the “no-penetration” condition. The boundary condition for the corresponding tangential velocity component is less obvious and has been the subject of ongoing debate since the 19th century [8,9]. The most common assumption is that the tangential fluid velocity matches that of the solid surface. This so-called “no-slip” boundary condition has become a central tenant of modern fluid mechanics, but everyday phenomena occur that are incompatible with this no-slip boundary condition [10]. One striking example is a droplet moving along a solid surface: the no-slip boundary condition at its three-phase contact line produces a stress (and force) singularity that prevents droplet motion if the no-slip boundary condition is applied, even though droplet motion is readily observed in nature. At single-nanometer length scales, nearly frictionless flow has been reported, e.g., through carbon nanotubes and other channels of nanometer size [11-13] implying considerable slip at the solid-liquid interface.

The Navier slip condition [14] is widely used to describe the presence of slip at the liquid/solid interface, i.e., motion of a liquid relative to an adjacent solid surface at their interface; see Figure 3. The Navier slip condition states that the tangential fluid velocity at the interface is proportional to the shear velocity gradient of the fluid. This condition is characterized by a slip length, b , which (for a flat solid surface) is the distance from the real solid surface to a hypothetical surface beneath the real surface at which the no-slip condition applies. Combining this Navier slip condition with the above-mentioned no-penetration condition gives the following result that holds for any surface geometry and flow:

$$[(\mathbf{v} - \mathbf{u}_s - 2b \mathbf{n} \cdot \mathbf{D}) \cdot (\mathbf{I} - \mathbf{nn})]_{\text{surface}} = \mathbf{0}, \quad (7)$$

where \mathbf{u}_s is the velocity of the real solid surface and \mathbf{n} is its surface normal vector.

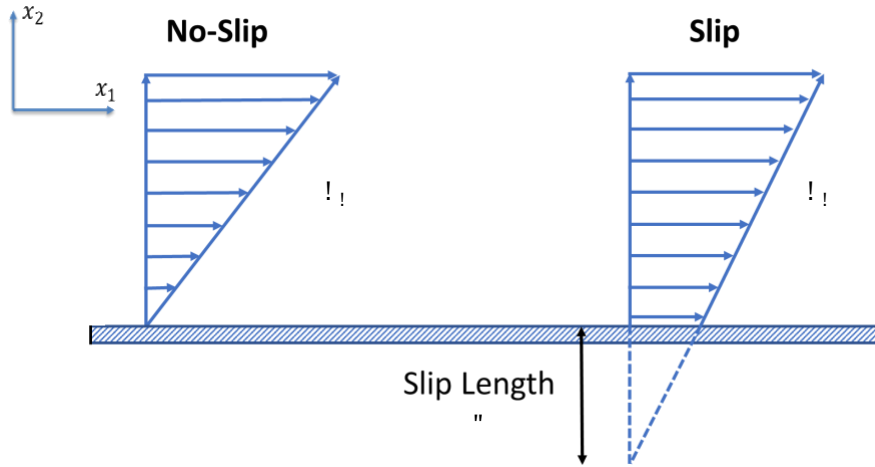


Figure 3. Illustration of the no-slip and Navier slip boundary conditions. The Navier slip condition corresponds to a velocity mismatch between the fluid flow and the plate. The slip length, b , is the projected length into the surface where the no-slip boundary condition is satisfied.

The no-slip boundary condition is recovered from Eq. (7) when the slip length, b , vanishes. Thus, if b is small relative to the characteristic length scale of the flow, Eq. (7) reduces to the no-slip condition. In practice, this assumption holds for macroscopic (everyday) flows of simple molecular liquids, such as water and glycerol. The no-slip condition is known to break down for small-scale flows of such liquids, with a wealth of molecular simulations and experimental data supporting slip on the nanometer scale [15-18].

We note that the Navier slip condition for gases can be derived from kinetic theory and the slip length related to the molecular mean free path in the gas. For liquids, theoretical studies are primarily based on molecular dynamics and arguments from linear response theory [19-22] providing an empirical connection to the underlying molecular processes. We note also that the mechanism for the nanoscale slip of simple liquids is different from the mechanisms responsible for the slip that has been observed in complex fluids. For example, effective slip in viscoelastic polymer melts arises due to disentanglement of polymer chains anchored to the surface from chains in the melt [22-27], and slip in viscoelastic two-phase mixtures arises from depletion of the high-viscosity phase near the surface [28]. Characterization of how slip occurs in simple molecular liquids requires quantitative measurements of this slip, but such measurements remain a significant

challenge, as evidenced by varying quantitative results in the literature using different techniques [17,18].

In this article, we review recent experimental efforts aimed at measuring and characterizing the flows generated by resonating nanoparticles in simple molecular liquids. The resulting flows involve picosecond timescales and nanometer length scales, necessitating the use of non-conventional approaches to their characterization. Ultrafast optical spectroscopy provides a solution to this challenge, accessing the required small size and ultrafast time scales.

II. Probing the viscoelasticity and slip of simple molecular liquids

Viscoelasticity and interface slip of simple molecular liquids have been extensively measured, with distinct advantages and disadvantages for each experimental method. The recently developed technique using vibrating metal nanoparticles complements these previous methods and opens new avenues of investigation.

A. Measurements of viscoelasticity

The molecular relaxation of simple liquids has been studied most extensively using optical and acoustic scattering techniques. One approach involves inelastic scattering and can use visible light (Brillouin scattering) [29], neutrons [30,31], or x-rays [32,33]. The inelastic-scattering spectra show peaks at particular scattering vectors and frequency shifts that correspond to the wavevectors and frequencies of acoustic waves in the liquid. The line shapes of these peaks are determined by the dynamic structure factor, which is equal to the Fourier transform of the autocorrelation function for density fluctuations in the liquid. In other words, the line shape of a peak at a given frequency, ω , depends on the relaxation dynamics of the liquid at that frequency; peaks for which $\omega\lambda \approx 1$ correspond to $De \approx 1$. Analysis of these peaks can thus be used to interrogate the liquid's viscoelastic response. These measurements yield detailed information concerning the liquid's relaxation times as a function of temperature and wavevector. However,

fitting of scattering line-shapes can be involved, and neutron or x-ray scattering experiments require access to sophisticated beamlines.

Complementary to these inelastic-scattering measurements is the more direct interrogation of liquid relaxation through the propagation of bulk ultrasonic waves. By measuring ultrasonic propagation velocities and attenuation lengths for different frequencies and temperatures, relaxation times have been obtained for glycerol [34] and glycerol-water mixtures [35]. These experiments provided quantitative characterization of the mechanical relaxation times. However, they were limited by the quartz-crystal oscillators used to generate the ultrasonic waves to sub-gigahertz frequencies, limiting measurement to relatively long relaxation times. More recently, gigahertz-frequency ultrasonic waves were generated by ultrafast heating of metal films with a pump laser pulse. The wave propagation constants were determined by Brillouin scattering from a second, time-delayed probe pulse (see Figure 4) [36]. In this way, viscoelastic effects were measured in glycerol [37] and across the transition temperature for a glass-forming liquid [38,39].

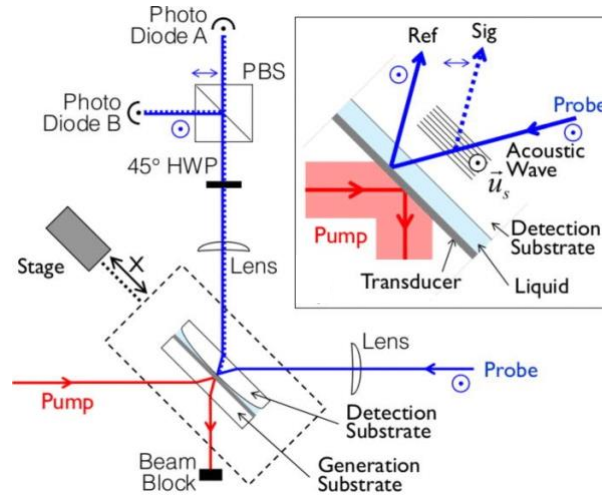


Figure 4. Setup for the measurement of gigahertz-frequency ultrasonic wave propagation in liquids. An ultrafast laser pump pulse sequence incident on a specialized shear transducer thin film launches both longitudinal and transverse acoustic waves into an adjacent liquid layer. After propagation through the liquid layer, the acoustic waves are detected in a transparent detection substrate by time-domain Brillouin scattering (Sig) of a tightly focused probe pulse, with direct reflection of the probe serving as a reference beam (Ref). The weak Brillouin-scattering signal is measured by balanced photodetection. Translation of the sample stage provides access to liquid layers with different thicknesses. From [37].

B. Slip measurements

The longest-standing technique for measuring slip in simple liquids involves the measurements of drainage forces, using either a surface force apparatus [40-43] or an atomic force microscope [44-49]. In both cases, one surface approaches a second surface with a liquid between the two. As the liquid is squeezed out, the resulting hydrodynamic flow exerts a force that depends on the slip length. Measurement of this drainage force can thus be used to infer the slip length [49], with resolution down to a few nanometers. However, various measurements using this method have resulted in different inferred slip lengths, raising concerns about potential experimental artifacts, such as surface deformations that can alter the flow [17,18]. Moreover, confinement effects at the small separations used can lead to structural reordering of the liquid molecules and violation of the underlying continuum assumption of the models used [50-52]. Indeed, the Navier slip condition implicitly assumes that the fluid away from the solid surface can be treated as a continuum.

Particle-tracking techniques directly interrogate slip in this unconfined regime [53-58]. This approach utilizes fluorescent probe particles that are suspended in the liquid and whose velocities are tracked by monitoring their optical emission. However, relatively large particles are required to provide sufficient fluorescent signal, limiting resolution to ~ 100 nm or greater [17,18].

In a new development [59], the hydrodynamics of individual nanoparticles were directly monitored as they flowed through a suspended microchannel resonator; see Figure 5. The hydrodynamic disturbance flow generated by the particle altered the resonance properties of the suspended resonator. By measuring these resonance properties in real time, repeating measurements on a single particle hundreds of times, and modeling the results using a statistical theory, precise measurements of the slip length on each particle were reported. Gold nanoparticles of identical surface treatment and different size, immersed in water, produced a constant Navier slip length of 2.7 ± 0.3 nm. This constancy in the slip length is aligned with the constitutive nature of the Navier slip length for a fixed surface/liquid system. Moreover, the particle diameters used were much smaller than the flow channel dimensions, ensuring the generated flows away from the particle surfaces satisfied the continuum hypothesis.

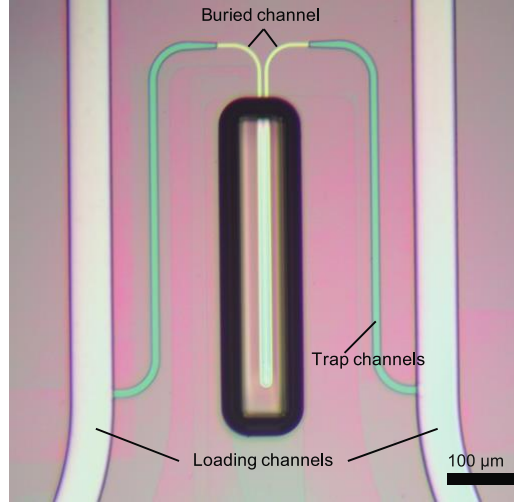


Figure 5. Optical-microscope image of the apparatus used to measure slip around suspended nanoparticles in a microchannel. Nanoparticles are passed one at a time through loading, trap, and buried channels into a suspended channel within the cantilever, which is enclosed in a vacuum chamber. From [59].

C. Nanoparticle vibration measurements

Time-domain measurements of nanoparticle vibrations are in many ways similar to the time-domain Brillouin-scattering measurements discussed above [60]. Rather than exciting acoustic waves in the liquid through the heating of a metal film, liquid flow is excited by impulsive heating and subsequent oscillation of metal nanoparticles suspended in the liquid. A probe pulse monitors the frequency and damping of the resulting nanoparticle oscillations. Since the frequency and damping depend on interaction between the vibrating nanoparticles and the surrounding liquid, the mechanical properties of the liquid and of the solid-liquid interface can be inferred [61]. By using nanoparticles with different geometries, radial or transverse vibrations can be excited, providing access to either compressive (longitudinal) or shear (transverse) motion. Moreover, by changing the nanoparticle size, vibration frequencies can be tuned from the GHz to the THz range [62,63]. This fills in the gap between the frequency ranges that can be accessed by ultrasonic and scattering techniques, providing direct access to viscoelastic effects in liquids with single-picosecond relaxation times (such as water).

By probing the mechanical interaction between the vibrating nanoparticle and the surrounding liquid, this technique provides information not only about the properties of the liquid but also about the solid-liquid interface. In particular, the same measurements that probe viscoelasticity in simple liquids also probe slip at the interface between these liquids and the solid surfaces of the nanoparticles. Moreover, as we show below, the nanoparticle-vibration measurements can be sensitive to slip at the single-nanometer scale.

A wide variety of solid nanoparticles with different sizes, shapes, and compositions can be dispersed as colloidal suspensions. Particles with diameters of 1 to 1000 nm exhibit mechanical vibrational resonance frequencies ranging from 1 THz down to 1 GHz, respectively. Exciting these nanoparticle vibrations thus produces ultrahigh-frequency flows in the surrounding liquid. The vibrations will be damped in part due to mechanical energy transferred from the nanoparticles to the surrounding liquid. Measuring the vibrational response thus provides information about the mechanical properties of the flowing liquid and the transfer of mechanical energy across the solid-liquid interface, in addition to energy dissipation processes interior to the particles themselves.

Elasticity of the surrounding liquid decreases the observed damping rate and increases the frequency of the vibration as compared to the case of a purely viscous liquid, due to enhanced stiffness of the particle / liquid system. Damping rates are often quantified using the dimensionless quality factor:

$$Q = 2\pi \frac{E_{\text{stored}}}{E_{\text{diss}}}, \quad (8)$$

where E_{stored} is the maximum elastic energy stored in the nanoparticle and its surroundings during a given oscillation cycle and E_{diss} is the energy dissipated in that cycle. As illustrated in Figure 6, for Newtonian liquids where $De \ll 1$, elastic energy is stored exclusively in the solid nanoparticle. By contrast, for liquids that display significant elasticity, $De \gtrsim 1$, substantial elastic energy is also stored in the liquid. Measurements of Q for particles in viscoelastic liquids will reflect this increased elastic energy storage. These measurements are most conveniently performed using the identity, $Q = \omega_{\text{res}}\tau/2$, where ω_{res} is the angular resonance frequency and τ is the time constant for decay of the nanoparticle oscillations.

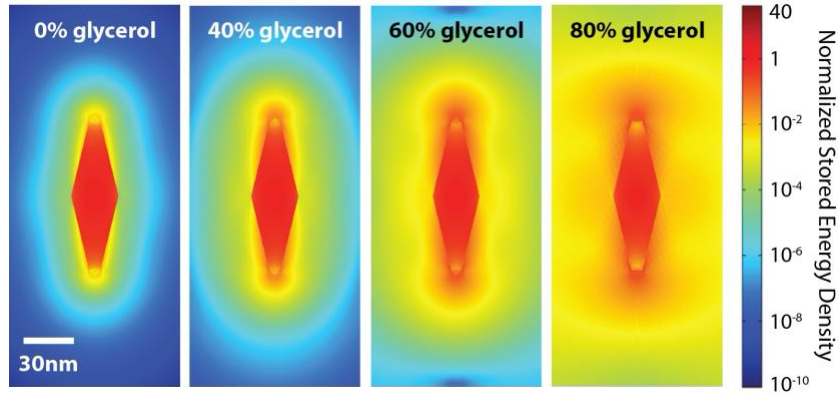


Figure 6. Calculated maximum energy density stored in a vibrating bipyramidal gold nanoparticle and in surrounding water-glycerol mixtures; for increasing glycerol fraction, the mechanical relaxation time of the liquid increases and the liquid displays greater viscoelastic behavior. The color scale indicates the stored energy density, normalized by the energy density in the center of the nanoparticle. From [64].

Velocity slip at the liquid/solid interface can cause an additional increase in Q for nanoparticle vibrations. Extensional vibrations of a rod-shaped nanoparticle generate a shear flow in the liquid, with the velocity for a Newtonian fluid decaying from the surface over a length scale given by the viscous penetration depth, $\delta = \sqrt{\mu/(\rho\omega)}$, where ρ is the fluid density. To illustrate this, consider a solid plate executing rectilinear oscillations in its plane, i.e., in the Cartesian x -direction, above which exists an unbounded Newtonian fluid (see Figure 3) [1]. Application of the no-slip boundary condition to the Navier Stokes equation gives the required velocity field,

$$\mathbf{u}(y, t) = u_s \exp\left(-i\omega t - C\frac{y}{\delta}\right) \hat{\mathbf{x}}, \quad (9)$$

where u_s is the speed amplitude of the lower plate, ω is the oscillation frequency, the constant $C = 1/\sqrt{2}(1 - i)$ where i is the imaginary unit, $\hat{\mathbf{x}}$ is the Cartesian basis vector in the x -direction, y is the Cartesian coordinate normal to the plate ($y = 0$) and t is time. Application of the Navier slip condition modifies Eq. (9), yielding [65]

$$\mathbf{u}(y, t) = U_s \frac{\exp\left(-i\omega t - C \frac{y}{\delta}\right)}{1 + C \frac{b}{\delta}} \hat{\mathbf{x}}. \quad (10)$$

This result shows that, while the distance dependence of the velocity field is unchanged, the magnitude of the fluid velocity at the plate decreases in the presence of slip. This in turn reduces the velocity gradient and hence the energy dissipated in the fluid. For nanoparticles vibrating in the gigahertz to terahertz regime, δ is at the nanometer scale, so that nanometer-scale slip lengths can appreciably reduce vibrational damping.

III. Optical Measurements of Metal-Nanoparticle Vibrations

The vibrations of nanoparticles are most commonly transduced and measured using optical techniques, because of their ability to combine noninvasive excitation and detection, high sensitivity, and access to picosecond time scales. Optical access to sub-wavelength sized metal particles is achieved via their plasmonic properties [66,67]. The oscillating electric field of an incident optical wave induces a collective oscillation of conduction electrons in the metal. This collective oscillation, known as a plasmon, allows the nanoparticle to strongly absorb and scatter the incident light, with an optical cross-section often orders of magnitude larger than the physical cross-sections of the particles.

A. Plasmon resonance of metal nanoparticles

The plasmon resonance frequencies of a nanoparticle depends primarily on its shape and composition. These frequencies can be calculated by treating the particle as a bulk metal with a complex frequency-dependent dielectric function [68]. For a classical Drude metal, the dielectric function is

$$\varepsilon(\Omega) = 1 - \frac{\Omega_p^2}{(\Omega^2 + i\Omega\gamma)}, \quad (11)$$

where Ω is the optical frequency, γ is the Drude damping rate, and $\Omega_p^2 = nq^2/m\epsilon_o$ is the bulk plasma frequency; here, n is the number density of electrons, q is the charge of an electron, m is

the electron mass, and ϵ_o is the permittivity of free space. This model does not consider interband transitions in the metal, which are most simply represented as a series of Lorentzian absorption peaks. This gives the Drude-Lorentz model:

$$\epsilon(\Omega) = \epsilon(\infty) + \Omega_p^2 \sum_{n=0}^N \frac{f_n}{(\Omega_{0,n}^2 - \Omega^2 - i\Omega\gamma_n)}, \quad (12)$$

where $\epsilon(\infty)$ is the high-frequency dielectric constant, f_n is the oscillator strength for the n^{th} Lorentzian term, $\Omega_{0,n}$ is the n^{th} interband transition frequency, γ_n is the damping rate for the n^{th} interband transition, and N is the number of oscillators.

For a spherical particle whose radius is much smaller than the optical wavelength, i.e., the quasi-static limit, the polarizability of the particle is

$$\alpha = V \frac{\epsilon(\Omega) - \epsilon_m}{\epsilon(\Omega) + 2\epsilon_m}, \quad (13)$$

where V is the particle volume, $\epsilon(\Omega)$ is the dielectric function of the metal, and ϵ_m is the dielectric function of the surrounding medium (assumed to be non-absorbing and frequency independent). Plasmon resonance occurs when $\text{Re}\{\epsilon(\Omega)\} = -2\epsilon_m$, i.e., in a region where the real part of Eq. (12) is negative. For silver and gold, the most commonly used materials for plasmonic nanoparticles, this occurs at visible wavelengths. The exact resonance condition depends on all the parameters in Eq. (13), including the electron density and the interband transition frequencies, all of which are characteristic of a particular metal.

For prolate ellipsoidal nanoparticles in the quasi-static limit, Eq. (13) becomes

$$\alpha = V \frac{\epsilon(\Omega) - \epsilon_m}{\epsilon_m + L [\epsilon(\Omega) - \epsilon_m]}, \quad (14)$$

for polarization along the long axis of the rod, and the geometric factor L depends on the particle's eccentricity, e (not the natural number):

$$L = \frac{1 - e^2}{e^2} \left(\frac{1}{2e} \ln \frac{1 + e}{1 - e} - 1 \right). \quad (15)$$

Elongating a spherical particle into a rod, i.e., increasing L , generally shifts the plasmon resonance condition to longer wavelengths. Determining resonance frequencies for more complex nanoparticle geometries requires numerical simulation, with particles generally supporting multiple plasmon resonances.

B. Raman scattering detection

The large polarizability of a nanoparticle at the plasmon resonance frequency enhances its optical cross-sections, not only of absorption and scattering, but also of higher-order processes such as Raman scattering. Although Raman scattering is most commonly used to probe vibrations in molecules and localized phonons in solids, it can also be used to probe the vibrational modes of nanoparticles [69-72]. Deformation of the nanoparticle due to mechanical oscillations significantly changes the polarizability of the particle near its plasmon resonance, resulting in a large Raman-scattering signal.

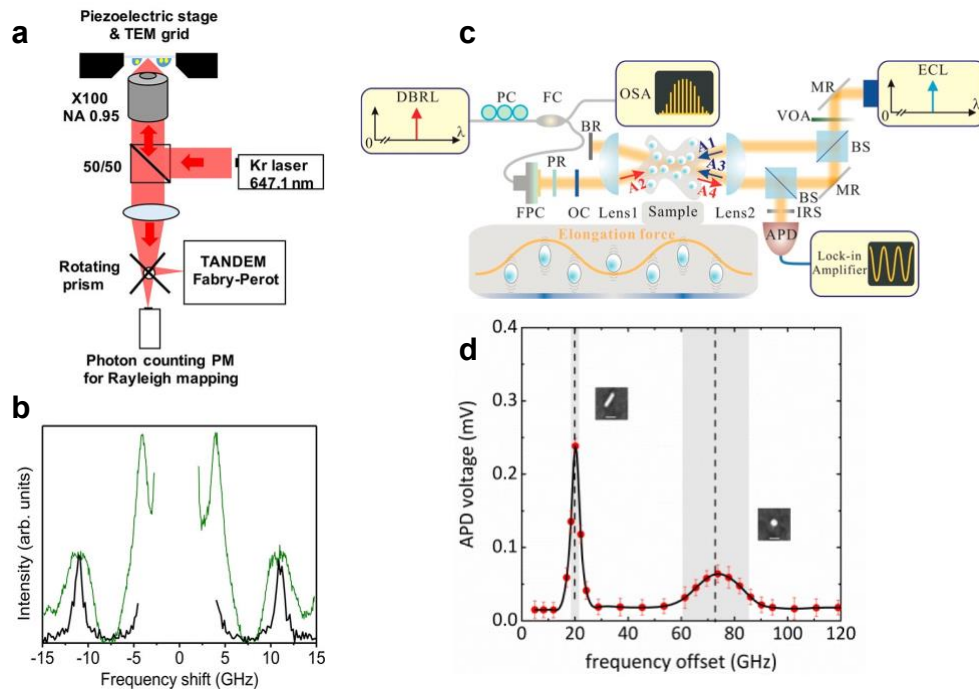


Figure 7. (a) Schematic of the experimental apparatus used to measure Raman scattering from individual metal nanostructures. Rayleigh scattering is used to locate individual particles, and a Fabry-Perot cavity is used to isolate their low-frequency Raman signal. (b) Raman scattering signal from a single 100-nm quasi-spherical gold nanoparticle (black line). The spectrum from an

ensemble of nanoparticles is shown for comparison (green line). From [78]. (c) Schematic of the apparatus used for continuous-wave four-wave-mixing measurements on nanoparticles. DBRL: distributed Bragg reflector laser; PC: polarization controller; FC: fiber coupler; OSA: optical spectrum analyzer; BR: blocker; FPC: fiber-port collimator; PR: polarizer; OC: optical chopper; IRS: iris; APD: avalanche photodetector; BS: beam splitter; MR: mirror; VOA: variable optical attenuator; ECL: external-cavity laser. From [78]. (d) Four-wave-mixing signal from a solution containing a mixture of rod-shaped and quasi-spherical gold nanoparticles. The dashed lines indicate the calculated resonance frequencies for extensional vibrations of the nanoparticles. From [79].

The polarizability change responsible for the Raman signal arises from two primary mechanisms: (1) changes in nanoparticle shape (e.g., see Eq. (14)), and (2) changes in local dielectric constant due to strain in the deformed nanoparticle [73]. For the second mechanism, the changes in dielectric constant arise from the deformation potential, or strain-induced changes in the metal's band structure; this can be represented as strain-dependent shifts in the interband transition frequencies, $\Omega_{0,n}$, in Eq. (12). For quasi-spherical nanoparticles, quadrupolar spheroidal vibrations produce large shape-induced changes in polarization, and these modes dominate the low-frequency Raman spectrum. Radially symmetric breathing modes couple to the plasmon polarization weakly through the deformation potential, and thus produce much weaker Raman lines [74,75]. For more complex nanoparticle geometries, strong Raman lines can be obtained for vibrations where the maximum deformation of the nanoparticle overlaps with the maximum of the confined optical field due to the plasmon [76].

The strong plasmonic enhancement of Raman signals from vibrating metal nanoparticles enables the characterization of vibrational modes even for dilute samples. Indeed, micro-Raman measurements have been able to resolve signals even from individual gold nanoparticles and nanoparticle dimers (see Figure 7a-b) [77,78]. The measured Raman shifts correspond to the resonance frequencies of the nanoparticle vibrational modes, and the linewidths provide information about the damping rate of these modes. Measuring Raman scattering from nanoparticles in liquid can thus, in principle, be used to probe the fluid-mechanical properties of the liquid.

C. Continuous-wave four-wave mixing detection

A second frequency-domain technique for measuring nanoparticle vibrations has also been developed recently, based on continuous-wave four-wave mixing (FWM) [79-82]. As illustrated in Figure 7c, a pump beam from a tunable laser (A2) interferes with a beam from a fixed-frequency laser (A3). The spatially varying optical field produced by this interference produces optical forces on the nanoparticles; the nanoparticle deformations produced by these forces result in local changes in the refractive index of the sample. The result is a traveling refractive-index grating, which diffracts a second pump beam (A1) that is also generated from the fixed-frequency laser. The diffracted signal (A4) is a maximum when the frequency difference between (A2) and (A3) matches the acoustic resonance of the nanoparticles. By sweeping the frequency of the tunable laser, then, the nanoparticle vibrations can be characterized in the frequency domain, with the center of the resonance giving the vibration frequency and the linewidth of the resonance providing the damping rate.

In the FWM experiments, the particles are deformed by the electrostrictive force produced by the optical field. This force elongates the particles in the polarization direction, so the measurements probe primarily extensional vibrational modes of the nanoparticles. This is in contrast to the quadrupolar modes that dominate in Raman spectroscopy, enabling the study of different modes of interaction between the vibrating nanoparticles and their surrounding environment. On the other hand, Raman scattering and FWM are both frequency-domain measurements for which precise measurements of the vibrational damping rates requires sufficient spectral resolution in the linewidths. Both experiments are also subject to a strong Rayleigh-scattering background, which especially complicates the measurement of low-frequency vibrations. These two techniques are thus best suited for the study of small particles with correspondingly high vibration frequencies and for the study of particles that experience strong vibrational damping.

D. Transient-absorption detection

For the study of larger nanoparticles or weaker vibrational damping, time-domain measurements present some advantages. Time-domain studies of metal-nanoparticle vibrations have generally involved the ultrafast pump-probe, or transient-absorption, technique [60,82-86].

In this technique, illustrated in Figure 8a, an ultrafast (sub-picosecond) “pump” laser pulse excites the sample, and a second (weaker) “probe” laser pulse passes through the sample after a controlled time delay. The transmission of the probe in the presence and absence of the pump are compared, and the change in transmission is recorded as a function of the pump-probe time delay.

In time-domain measurements of metal-nanoparticle vibrations, the purpose of the pump pulse is to increase the nanoparticle temperature via optical absorption. The pump wavelength is therefore often tuned to match the plasmon resonance frequency, although it can also be tuned to shorter wavelengths where interband absorption is strong. The energy from the absorbed photons is initially transferred to electrons in the metal, but this energy is rapidly transferred to the lattice, on time scales less than 10 ps [87,88]. The pump-pulse absorption thus leads to the nearly impulsive heating and thermal expansion of the nanoparticle. This expansion, in turn, excites vibrational modes; because the modes are excited by thermal expansion, primarily centrosymmetric modes are studied by the pump-probe technique [89]. (Non-centrosymmetric modes can be excited if there are sufficient asymmetries in laser incidence or in material properties [90].) For spherical particles, the centrosymmetric modes are the radial breathing modes, but extensional modes can also be excited by thermal expansion in anisotropic nanoparticles.

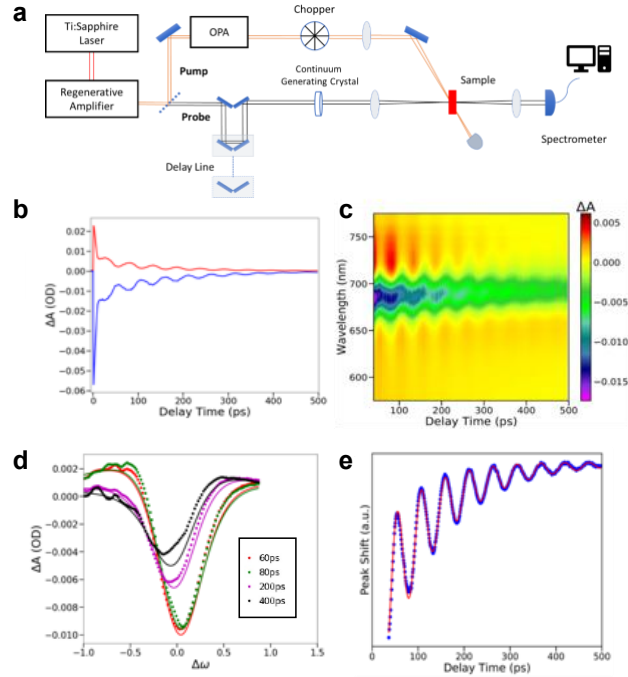


Figure 8. (a) Schematic of a typical transient-absorption apparatus. Ultrafast, high-intensity laser pulses (generated, in this case, by a mode-locked titanium-sapphire laser and a regenerative amplifier) are divided into a pump and a probe pulse. The frequency of the pump is often converted (here, using an optical parametric amplifier) to match the desired excitation frequency. The probe is delayed relative to the pump, and its transmission through the sample is measured as a function of the pump-probe delay time. In this setup, the probe is focused into a nonlinear crystal to generate a broadband pulse, and the transmission of the probe is resolved as a function of wavelength using a spectrometer. The chopper enables the probe transmission with and without the pump to be compared. (b-e) Representative transient-absorption data for vibrating metal nanoparticles. (b) Selected changes in extinction as a function of pump-probe delay time, for probe wavelengths longer (red) and shorter (blue) than the plasmon resonance wavelength. (c) Extinction change as a function of probe wavelength and of pump-probe delay time. (d) Selected changes in extinction as a function of probe wavelength, for different pump-probe delay times (points). Also shown are fits of these transient spectra to the difference between two Lorentzian functions (lines). (e) Fractional plasmon peak shift as a function of pump-probe delay time, determined by fitting transient spectra (points). Also shown is a fit to a decaying oscillation on top of a decaying exponential background (line).

The vibrations of the nanoparticles modulate the plasmon resonance frequency of the nanoparticles; in addition to the changes in nanoparticle shape and the deformation potential that are primarily responsible for Raman signals, the frequency modulation in transient-absorption experiments also arises from local changes in electron density (which change the bulk plasmon frequency, Ω_p , see Eq. (12)) [91]. The contribution of each mechanism to the overall shift in the plasmon resonance is dependent on the shape, material, and vibrational mode excited, with the largest shifts again observed when the maximum in local strain overlaps with the maximum in the localized optical field. As the plasmon resonance frequency oscillates, extinction of the probe pulse near the plasmon resonance frequency oscillates, and this oscillation in probe transmission can be used to monitor the nanoparticle vibrations, including their frequency and damping rate.

The periodic change in transmission is greatest a half-width-at-half-maximum away from the plasmon resonance frequency, so probe wavelengths slightly shorter or slightly longer than the resonance wavelength are commonly used to monitor nanoparticle vibrations (see Figure 8b). However, the oscillations in plasmon resonance wavelength due to mechanical vibrations are accompanied by a decaying shift in the resonance due to the impulsive heating of the metal lattice and subsequent cooling by heat transfer to the surroundings (generally on time scales of 10 – 1000 ps). This shift will cause slightly faster decay of the signal for probe wavelengths on one side of the resonance as compared to the other, leading to small but systematic errors in the measured mechanical quality factors. To avoid this artifact, a broadband probe pulse can be used, and the extinction can be resolved as a function of wavelength for each pump-probe delay time (see Figure 8c). Each of these transient spectra can be fit to a difference in Lorentzians, comparing the extinction of the excited nanoparticles to the ordinary, linear extinction of the nanoparticles (see Figure 8d). From these fits, the time-dependent shift in plasmon resonance frequency, $\Gamma_p(t)$, is obtained (see Figure 8e) [92].

IV. Liquid Damping of Nanoparticle Vibrations

Using nanoparticle vibrations as a probe of nanoscale liquid dynamics requires the ability to measure the frequency and damping rate, or quality factor, of the vibrations. In practice, measurement of the latter quantity is complicated by the variation in the size and shape of the

nanoparticles that make up any given sample. Nanoparticles with slightly different dimensions will vibrate with slightly different frequencies. For frequency-domain measurements, this leads to an inhomogeneous broadening of the resonance line. For time-domain measurements, it leads to an inhomogeneous dephasing of the oscillations. For early measurements of nanoparticle vibrations, these inhomogeneous effects dominated the measurements, masking any damping due to the mechanical response of the nanoparticles, and thereby making it impossible to measure the true mechanical quality factors.

One approach to overcoming the effects of inhomogeneous broadening is to take measurements on single nanoparticles [93,94]. In the first time-resolved measurements of nanoparticle vibrations, the particles were deposited at a low density on substrates, so that they could be individually imaged in an optical microscope. The pump and probe beams were then focused through the microscope objective onto the isolated single nanoparticles, and transient signals were collected in transmission or reflection. The main challenge in these experiments was obtaining a sufficiently high signal-to-noise ratio. The extinction cross-section of a single particle is only a small fraction of even a diffraction-limited laser spot size, and vibrations produce a relatively small modulation of this extinction cross-section. The single-particle measurement must therefore be able to resolve relative extinction changes significantly smaller than 10^{-4} in order to accurately measure nanoparticle vibrations. A number of signal-enhancing methods have been developed for these measurements, including interferometry [95] and high-speed lock-in detection [96,97].

The interaction between the vibrating particles and a liquid environment can be measured by placing a drop of liquid on top of the nanoparticle-carrying substrate. The first such measurements involved nanofabricated gold nanorings on quartz substrates [98]. As shown in Figure 9a-b, the quality factor for the axisymmetric breathing mode decreases significantly when the nanorings are immersed in glycerol. This indicates that, for the nanorings in glycerol, most of the mechanical damping comes from viscous dissipation in the liquid environment, with only a secondary contribution from mechanical coupling between the nanorings and the substrate. However, significant variation is seen in measured damping rates; this has been tentatively attributed to varying mechanical contact between the nanoring and the substrate [99] but may also arise from differences in microstructure among the polycrystalline structures involved.

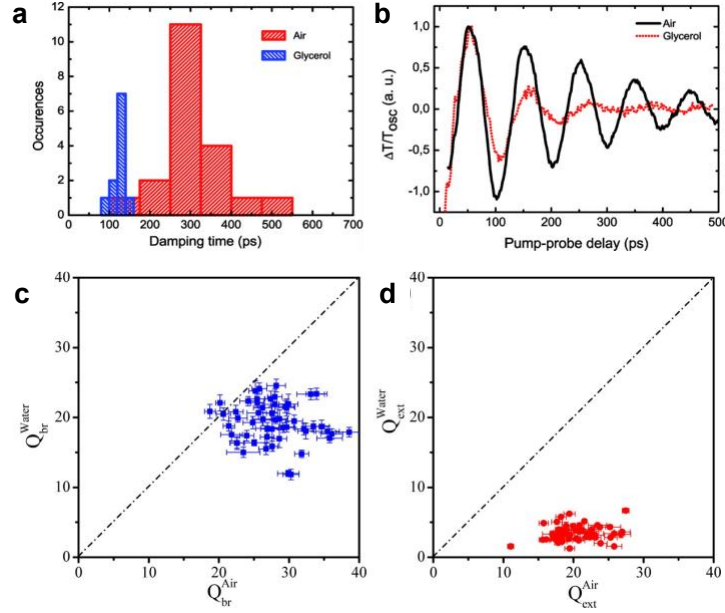


Figure 9. (a-b) Damping of breathing modes for individual microfabricated gold nanorings, measured by single-particle pump-probe spectroscopy. (a) Damping time distribution measured in two different media: air and glycerol. (b) Sample oscillating component of the probe signal for a vibrating gold nanoring in air (solid line) or glycerol (dashed line). From Ref. [98]. (c-d) Quality factors for the vibrations of individual chemically synthesized gold nanorods, measured by single-particle pump-probe spectroscopy, for (c) the breathing mode of the nanorods, and (d) the extensional mode of the nanorods. From [100].

A later study involving chemically synthesized gold nanorods deposited on a glass substrate again showed a decrease in quality factor when the samples were immersed in liquid (in this case, water), also with a significant variation in the measured quality factors (see Figure 9c-d) [100]. The structural identity among the nanorods suggests that this scatter is indeed primarily due to variations in nanorod-substrate coupling. Interestingly, the damping of the extensional vibrational mode of the nanorods by the surrounding water is significantly greater than that of the breathing mode. This was attributed to hydrodynamic lubrication forces between the particle and the substrate (that is, to the flow of the water confined in the thin gap between the solid particle and the solid surface below).

These experiments illustrate the central challenge of using the vibrations of single particles to probe nanoscale fluid dynamics: the particles must be immobilized for the duration of the measurement (generally several minutes or longer). Depositing the particles on a substrate

complicates the study of the particle-liquid interaction due to the particle-substrate interaction. This challenge was overcome by optically trapping individual nanoparticles while measuring their vibrations (see Figure 10a) [101]. This method represents perhaps the ideal means to probe high-frequency structure-liquid interaction at the nanoscale, but also represents a significant experimental challenge.

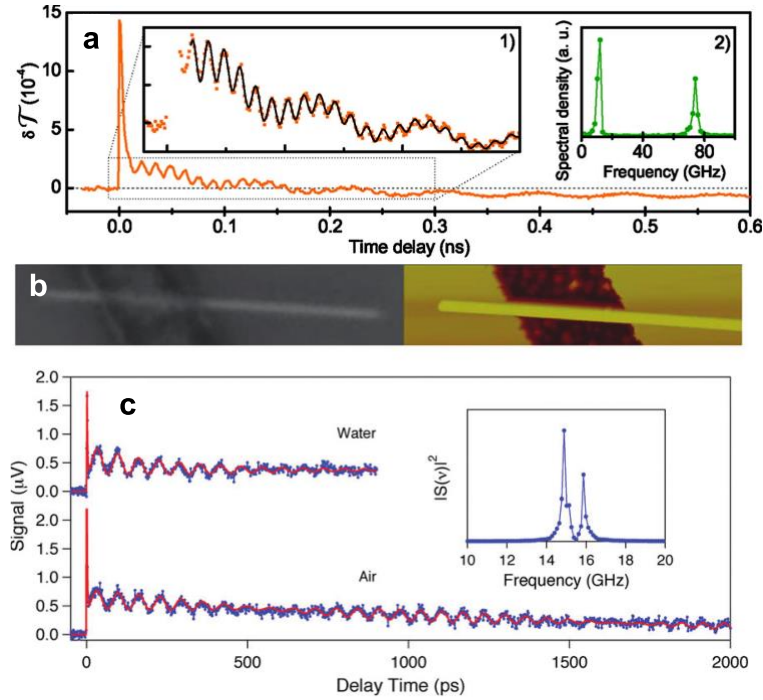


Figure 10. (a) Probe signal from a pump-probe experiment on a single gold nanorod optically trapped in water. Inset (1) shows an expansion of part of the time trace, and inset (2) shows the power spectral density of the oscillatory portion of the time trace. From Ref. [101]. (b-c) Pump-probe measurements of breathing-mode vibrations of a single gold nanowire suspended above a trench. (b) Scattered-light and atomic-force-microscope images of a suspended nanowire. (c) Probe signal for the vibrating nanowire in water and in air. The inset shows the power spectral density of the time trace. From Ref. [102].

A somewhat more manageable method to overcome substrate interactions involves measuring the breathing-mode vibrations of single gold nanowires suspended over a trench in a substrate [102]. These vibrations in the suspended portion of the nanowire are nearly entirely decoupled from the substrate. The same nanowire can be measured when it is suspended in air and when it is immersed in water (see Figure 10b-c). The quality factor for the vibrations in air is almost entirely due to mechanisms other than the air-structure interaction, i.e., energy loss within

the nanowire itself (including any adsorbed molecules on its surface and coupling to the mounting substrate); this is commonly termed the “intrinsic” quality factor, Q_{int} . The quality factor for the vibrations in water, Q_{tot} , includes both intrinsic damping and damping due to the surrounding liquid environment, Q_{env} :

$$\frac{1}{Q_{\text{tot}}} = \frac{1}{Q_{\text{env}}} + \frac{1}{Q_{\text{int}}}. \quad (16)$$

By comparing the measurements in air and water, then, the specific rate at which energy is transferred from the vibrating nanowire to the surrounding water can be determined quantitatively. Comparison to theory indicates that transfer of energy to the water occurs mainly through the generation of outgoing sound waves. This is expected for the breathing modes that are probed in these measurements, because the mostly radial motion of the nanowire surfaces primarily induces compressional flow in the surrounding liquid.

The purpose of the single-particle experiments is to overcome the inhomogeneous broadening or dephasing that comes from variations in the dimensions of nanoparticles in the ensemble. An alternative strategy is to use ensemble measurements on samples of nanoparticles with very high monodispersity. This has recently become a viable strategy, with the advent of colloidal-synthesis methods that lead to highly uniform samples of gold nanoparticles with narrow particle size distributions (see Figure 11). For these samples, the measured probe signal will have the form [103]:

$$\Gamma_p(t) = A_0 \exp\left(-\frac{t}{\tau_{\text{tot}}}\right) \exp\left(-\frac{t^2}{\tau_{\text{inh}}^2}\right) \sin(\omega t + \varphi) + A_1 \exp\left(-\frac{t}{\tau_{\text{cool}}}\right), \quad (17)$$

where symbols are defined in the following text. Here, we have considered the signal to be the time-dependent shift in the plasmon resonance frequency, $\Gamma_p(t)$ (as discussed above, this removes artifacts associated with measurements involving a single probe wavelength). The second term accounts for the contribution due to heating of the lattice and subsequent exchange of that heat with the surroundings, with time constant τ_{cool} ; A_0 and A_1 are constants that account for the relative contributions of the oscillatory and thermal mechanisms. Energy damping, including both

intrinsic and liquid damping, is described by $\tau_{\text{tot}} = 2Q_{\text{tot}}/\omega_{\text{res}}$. The mechanical resonance frequency, ω_{res} , is obtained from the measured vibrational frequency, ω , as

$$\omega_{\text{res}} = \omega \left(1 - \frac{1}{4Q_{\text{tot}}^2} \right)^{-\frac{1}{2}}. \quad (18)$$

Inhomogeneous dephasing is described by τ_{inh} ; if the vibrational period of a particle is proportional to its size dimension, L , and if that dimension is normally distributed with a mean L_0 and a standard deviation σ_L , then [103]

$$\tau_{\text{inh}} \approx \frac{\sqrt{2}L_0}{\omega\sigma_L}. \quad (19)$$

The parameters, L_0 and σ_L , can be determined by measuring the distribution of nanoparticle dimensions in electron-microscope images; τ_{inh} is thus known and does not have to be treated as a free parameter when fitting data to Eq. (17). The fits are therefore able to give robust values for both Q_{tot} and ω_{res} . These fits are generally applied to time series signals that start at pump-probe delay times of several picoseconds, to avoid the initial ultrafast signal due to heating of electrons in the nanoparticles [87,88].

The first measurements of the vibrations of highly monodisperse metal nanoparticles involved bipyramidal gold nanoparticles [104,105]. These particles are grown using a seed-mediated procedure that leads to five regular facets defining each of the ends of the bipyramid (see Figure 11a) [106]; the fixed structural geometry of the particles results in exceptional monodispersity in their length (as low as 2%). Pump-probe experiments are primarily sensitive to extensional vibrations of the bipyramids, whose periods are proportional to the particle length; inhomogeneous dephasing is thus weak in these experiments, enabling Q_{tot} to be determined. One detail worth noting is that the measured Q_{tot} was observed to increase with increasing pump power; the measurements were therefore repeated for several pump powers and the results were extrapolated to zero power.

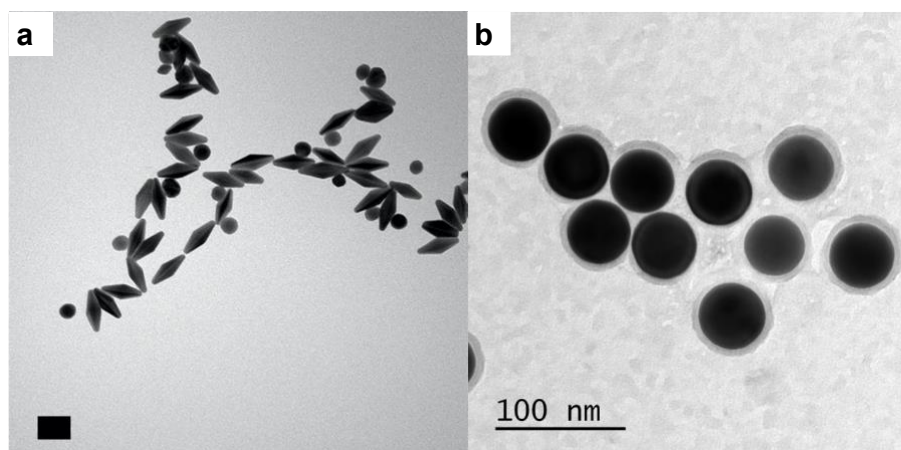


Figure 11. Representative transmission-electron-microscope image of highly monodisperse (a) bipyramidal and (b) spherical gold nanoparticles.

Several samples of gold bipyramids were each suspended in different liquids. As shown in Figure 12a, the energy damping rate scaled approximately as the square root of the liquid viscosity, μ , indicating that energy is transferred from the vibrating nanoparticles to the liquids primarily through viscous damping. This is expected for the longitudinal vibrations that are measured, because the faces of the particle mainly oscillate laterally, which produces a shear flow in the surrounding liquid. The figure also shows a comparison to a more detailed analytical model based on the approximation that the lengths of the bipyramids are much greater than their widths. In this comparison between theory and experiment, the intrinsic quality factor, Q_{int} , due to damping processes occurring within the nanoparticles is treated as a fitting parameter.

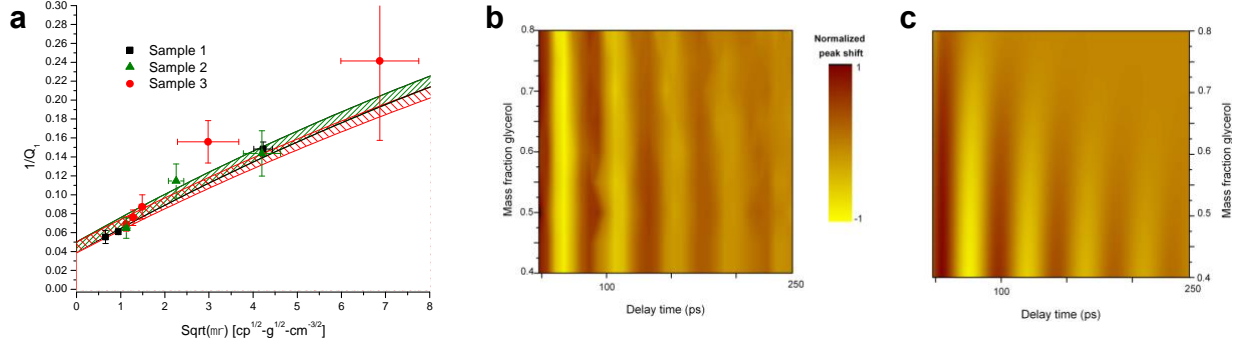


Figure 12. (a) Relationship between the total quality factor, Q_{tot} for the extensional vibrations of three different samples of bipyramidal gold nanoparticles in liquids with different shear viscosities, μ , and densities, ρ . Points are experimental values and dashed areas are theoretical fits based on an analytical model assuming viscous damping by Newtonian liquids. The range of the dashed areas corresponds to the range of intrinsic quality factors used in fitting theory to experiment. From [105]. (b-c) Comparison between experiment (b) and analytical simulations (c) for bipyramidal gold nanoparticles vibrating in liquids with different viscosities. The viscosity is varied by controlling the mass fraction of glycerol in glycerol-water mixtures, with higher glycerol content corresponding to higher viscosity. The calculations assume viscous damping in a Newtonian liquid. From Ref. [64].

V. Viscoelasticity of Simple Liquids: Probing Molecular Relaxation Using Nanoparticle Vibrations

Although the comparison between theory and experiment in Figure 12a clearly shows that viscous damping dominates the fluid-structure response for bipyramidal gold nanoparticles vibrating in simple liquids, discrepancies appear between the measured and calculated values. One limitation is that the theory does not consider the finite region over which viscosity acts on the

nanoparticles. This can be overcome by using numerical calculations that account for the measured nanoparticle geometry [107]. Finite-element simulations predict lower quality factors than the analytical model, due to end effects of the nanoparticles ignored in the model. However, this increases the disagreement between theory and experiment: for high-viscosity liquids, experiments show underdamped vibrations (Figure 12b) whereas the calculations in Figure 12c predict overdamped vibrations. This qualitative difference is consistent with the presence of viscoelastic effects in the liquids: as described above, this viscoelasticity will reduce the effect of damping of the nanoparticle vibrations by storing elastic energy in the liquid.

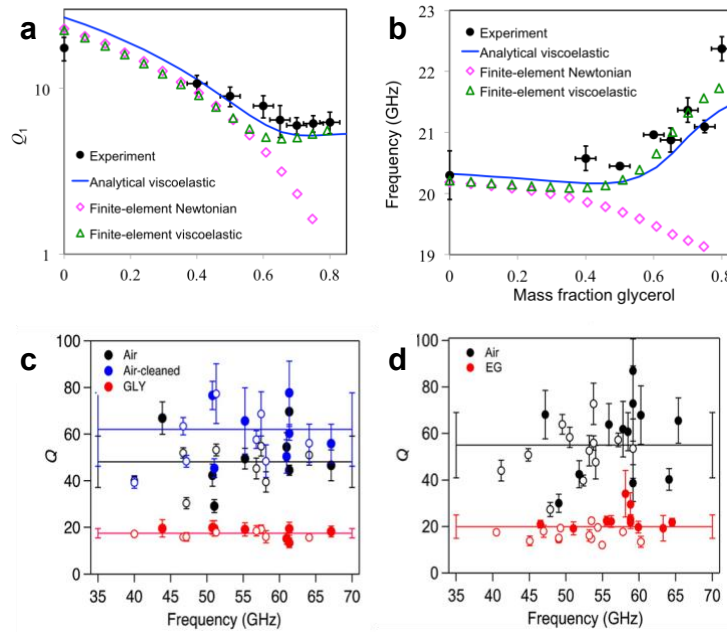


Figure 13. (a-b) Measured quality factors (a) and resonance frequencies (b) for the extensional vibrational modes of an ensemble of bipyramidal gold nanoparticles in a series of water-glycerol mixtures with different glycerol concentrations. For high glycerol concentrations, the vibrational period of the particles is comparable to the relaxation time in the liquid, and viscoelastic effects are observed. Experimental data (black circles) are compared to analytical and finite-element (FE) models for viscoelastic fluids and FE models for Newtonian fluids. From [64]. (c-d) Measured quality factors for the radial vibrational modes of single suspended gold nanowires in air before and after plasma cleaning and immersed in (c) glycerol or (d) ethylene glycol. Open symbols correspond to the low-frequency mode and closed symbols correspond to the high-frequency mode. From Ref. [108].

To determine whether viscoelasticity in the surrounding liquid is indeed influencing the nanoparticle vibration, measurements were made on bipyramidal gold nanoparticles in a series of water-glycerol mixtures [64]. These experiments clearly showed a plateau and even an increase in Q_{tot} with increasing glycerol concentration, as expected for viscoelastic fluids, and in clear contrast to predictions for Newtonian fluids (see Figure 13a). Moreover, these experiments were able to resolve changes in ω_{res} and showed an increase in resonance frequency with increasing glycerol concentration; this is the opposite to what would be predicted for viscous damping alone (see Figure 13b).

The analytical and finite-element models previously developed to describe the viscous damping of these nanoparticle vibrations were extended to treat the surrounding liquids as viscoelastic fluids using a linear Maxwell model. As shown in Figure 13a-b, the experimental data are in good agreement with the viscoelastic models and disagree qualitatively with the Newtonian model. In these experiments, as in the previous nanoparticle-ensemble measurements of viscous damping, the intrinsic damping, Q_{int} , is an adjustable parameter used to fit theory to experiment; this is a disadvantage as compared to the suspended-nanowire experiments, where Q_{int} can be independently measured using nanowires suspended in air.

Following the measurements with bipyramidal gold nanoparticles, viscoelastic effects in surrounding liquids were investigated using the radial vibrations of suspended gold nanowires [108]. Measurements were made in liquid environments with relatively high viscosities and long mechanical relaxation times, including glycerol, ethylene glycol, and a series of ionic solvents. By comparison to nanowires vibrating in air, Q_{env} was directly determined for several nanowires with different diameters in each of the solvents. These measured quality factors were higher than those calculated assuming a Newtonian response of the surrounding liquids, indicating that viscoelastic effects were in fact significant. Approximate agreement was obtained by modeling the liquids using a linear Maxwell model.

However, it was possible to describe the measured quality factors by simply assuming that the nanowires are vibrating in inviscid (zero-viscosity) compressible fluids, and that liquid damping is entirely due to the generation of outgoing sound waves [109]. This surprising result

was explained by considering that the nanowire vibrations had frequencies that probed the liquids in the highly elastic regime, $De \gg 1$. Intuitively, the response of the liquid is dominated by elastic effects in this regime, and the viscosity of the liquid is unimportant. Quality factors are thus independent of viscosity, and the response appears to be the same as that of an inviscid liquid. This simple intuition was supported quantitatively by both analytical models and finite-element simulations [110].

Within the contexts of either the inviscid or fully elastic descriptions, and within the measurement scatter, the experiments on gold nanowires agreed quantitatively with theory (see Figure 13c-d). This is in contrast to the measurements on bipyramidal gold nanoparticles, where there is a small but systematic deviation between the experimental values and theoretical predictions (see Figure 13a-b). As explained above, the deviation would be consistent with slip at the nanoparticle surfaces: interfacial slip reduces the coupling between the vibrating nanoparticle and the surrounding liquid, thus reducing damping and increasing Q beyond the predicted values based on models without slip. Since the vibrations of the nanowires are primarily radial, the effect of interfacial slip would be expected to be much lower, potentially explaining the improved agreement in this case. On the other hand, the nanowire-vibration measurements probe the liquids in the fully elastic regime, while the bipyramid vibrations probe the viscoelastic regime; in principle, this difference could play a role in the different levels of agreement between theory and experiment. For example, the Maxwell model used to describe the viscoelastic response of the liquids included only a single relaxation time, while it is known that a spectrum of relaxation times is required to properly describe their viscoelastic response; the effect of a relaxation-time spectrum would be apparent only for $De \sim 1$.

There was thus a need to make measurements that exclude the effects of slip and still probe the viscoelastic regime. That is, measurements were needed where the nanoparticle vibrations induce only a compressional flow of the surrounding liquid, and there is no shear motion of the nanoparticle surfaces in the liquid. At the same time, the vibrational frequencies needed to be in the range where $De \sim 1$. One nanostructure that can satisfy these conditions is a metal nanoplate, a chemically synthesized nanostructure with a thickness on the order of 100 nm and with lateral dimensions of several μm [111]. These nanoplates can be suspended over trenches or holes in substrates and the vibrations of the suspended portions can be measured by microscopic pump-

probe spectroscopy, as for the suspended nanowires. The vibrational modes excited and detected correspond to oscillations in the thickness of the nanoplates and can have high Q_{int} [112]; unlike the nanowire vibrations, the nanoplate vibrations have frequencies that can access the viscoelastic crossover regime, $De \sim 1$. These thickness oscillations can excite compressional waves in the fluid above and / or below the nanoplate, and are thus the ultra-high-frequency analogue of the ultrasonic transducers used for the first measurements of viscoelasticity in simple liquids [34,35]. In fact, the outgoing waves can be measured using time-domain Brillouin scattering [113], in analogy to previous time-resolved measurements of viscoelastic effects in ultrasonic wave propagation [36-39].

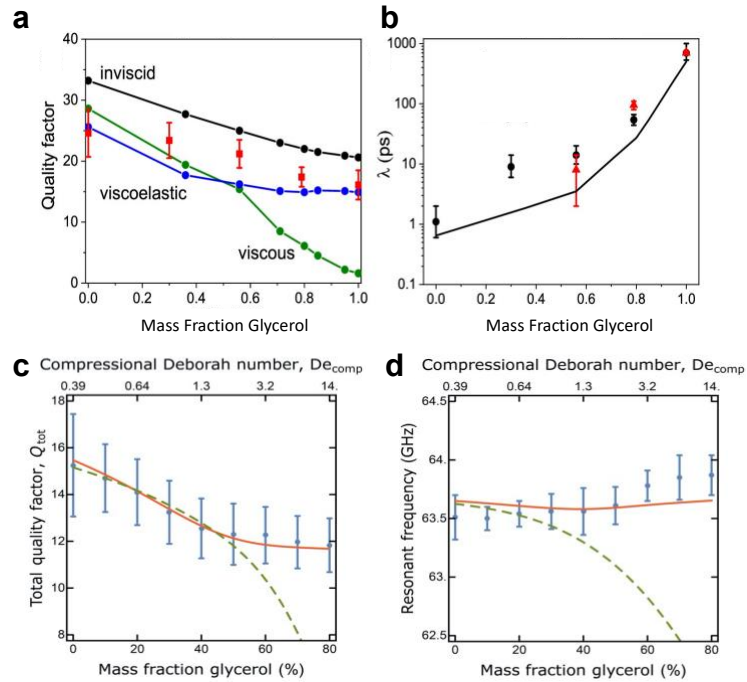


Figure 14. (a-b) Viscoelastic effects in water-glycerol mixtures probed by the thickness vibrations of suspended gold nanoplates. (a) Measured quality factors for the nanoplate vibrations for different glycerol mass fractions (red circles) and predictions assuming viscoelastic, viscous (Newtonian), and inviscid behavior of the surrounding liquids. The viscoelastic model in this case uses literature values for relaxation times. (b) Relaxation times, λ , for different glycerol mass fractions inferred from measurements of quality factors (black points) and from time-domain Brillouin-scattering measurements of sound speed (red points), together with literature relaxation times (line). From [114]. (c-d) Viscoelastic effects in water-glycerol mixtures probed by the radial vibrations of highly spherical gold nanoparticles. Measured quality factors (c) and frequencies (d) for different glycerol fractions (points) and predictions assuming viscoelastic

(solid red line) and Newtonian (dashed green line) behavior of the surrounding liquids. The compressional Deborah number, De , is given on the upper horizontal axis, showing that viscoelastic effects arise when $De \sim 1$. From [117].

The nanoplates thus provide two methods to probe viscoelastic effects in surrounding liquids: through the damping of the nanoplatelet vibrations and through the propagation of the outgoing sound waves [114]. As shown in Figure 14a, the experimental quality factors (averaged over measurements on several individual platelets) show a plateau with increasing mass fraction of glycerol, characteristic of viscoelastic behavior. The time-resolved Brillouin-scattering measurements give sound speeds at high glycerol concentration significantly higher than known values at lower frequencies, again consistent with a viscoelastic “stiffening” of the liquids. Comparison to a model that accounts for viscoelastic fluid behavior provides good agreement with the data (see Figure 14a-b). Discrepancies remain, as for the measurements on bipyramidal nanoparticles. In this case, however, the discrepancies may be due to limitations of the viscoelastic model, which assumed that the compressional relaxation time, λ_{comp} , is equal to the shear relaxation time, λ_{sh} (see Eq. (10)).

Another nanoparticle geometry that produces purely compressive flows is a sphere: pump-probe spectroscopy interrogates the breathing modes of these particles, which involve purely radial motion. Many of the earlier measurements of metal-nanoparticle vibrations involved nominally spherical nanoparticles [60,82-86]; however, the samples used in these experiments had irregular, faceted geometries. This meant a large variation in nanoparticle geometry from one particle to another, and thus significant inhomogeneous broadening. Even when this inhomogeneity was overcome, as in single-particle measurements [101], the faceted shape of the nanoparticles meant that their vibrations still involved shear motion, and their irregular and unpredictable shapes complicated comparison with theoretical models. Recent advances in colloidal synthesis techniques, however, have led to the ability to produce monodisperse samples of highly spherical gold nanoparticles (see Figure 11b) [115,116], providing a model system for nanoparticle-ensemble measurements of purely compressive flows.

As illustrated in Figure 14c-d, measurements on these highly spherical gold nanoparticles in glycerol-water mixtures with different glycerol content show the same qualitative features of viscoelastic fluid behavior as previously observed for bipyramidal gold nanoparticles: a plateau in

the quality factor and an increase in the resonance frequency with increasing glycerol content [117]. The spherical symmetry of the particle enables the expected frequencies and damping rates to be calculated using an analytical eigenvalue equation, without the need for numerical simulations. Predictions using the constitutive relations for a compressible Newtonian fluid (Eq. (9)) show significant qualitative deviations from experiment, whereas predictions using a linear Maxwell model for a compressible viscoelastic fluid (Eq. (10)) agree quantitatively with the experimental data (see Figure 14c-d).

Importantly, there is no longer a discrepancy between the measured data for the oscillation of highly spherical nanoparticles and the predictions of a linear Maxwell model, as there was for the oscillation of bipyramids (Figure 13c-d) and nanoplates (Figure 14a-b). This indicates, first, that the constitutive equations proposed in Ref. [5] provide an accurate description for the high-frequency flow of these simple liquids. The theory-experiment agreement for nanospheres, where shear motion is absent, also strongly suggests that the disagreement observed for bipyramids is due to slip at the solid-liquid interface, which can occur only in the case of shear motion.

VI. Viscoelastic Enhancement of Nanoscale Slip at the Solid-Liquid Interface

The quantitative understanding of compressible viscoelastic flows in simple liquids at the nanoscale motivates a re-examination of shear flows where slip can play a role. Experimentally, this means a re-examination of the extensional vibrations of bipyramidal gold nanoparticles in liquids (which produce shear flows) to examine whether slip can account for the previously observed differences between theory and experiment (see Figure 13b-c). Since these differences are relatively small, a wider dataset was measured, covering not only water-glycerol mixtures with different glycerol fractions but different temperatures for each of the mixtures [65]. For a given glycerol concentration, reducing the temperature increases the mechanical relaxation time of the liquid, increasing De . Temperature and composition tuning thus provide two separate means of crossing between the Newtonian and viscoelastic regimes.

To quantify the effect of slip, the finite-element calculations previously used to model bipyramid vibrations in viscoelastic fluids were further adapted to include slip at the interface,

using the Navier slip condition, Eq. (7). There are now two fitting parameters to compare theory and experiment: Q_{int} , as before, and the slip length, b (see Eq. (7)). These two parameters were obtained by fitting to the temperature-dependent data for a low glycerol concentration, where the fluid is Newtonian. These fitted parameters were then used without further adjustment to model the experimental data for all other glycerol concentrations. As shown in Figure 15, the model combining viscoelasticity and slip agrees quantitatively with the data for all glycerol concentrations and temperatures. It provides a good representation of the complete dataset, with the no-slip viscoelastic model predominantly underestimating the measurements.

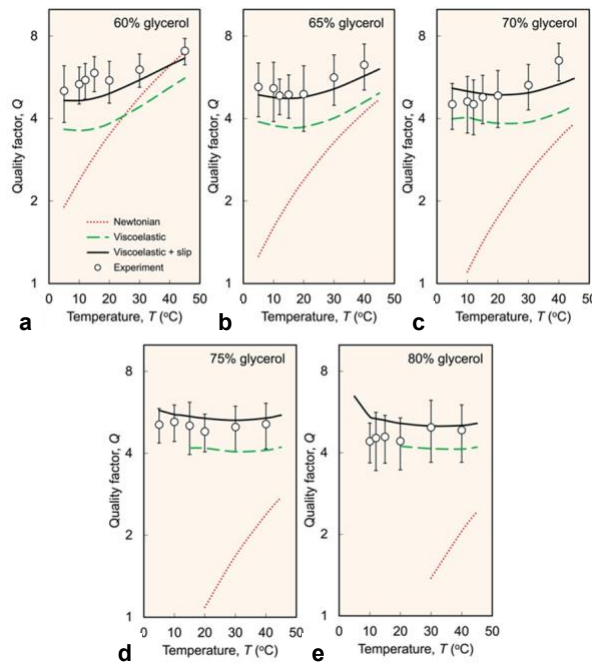


Figure 15. Measured quality factors for the extensional vibrations of bipyramidal gold nanoparticles in water-glycerol mixtures with different mass fractions of glycerol, as a function of temperature, together with (i) theoretical predictions assuming Newtonian behavior of the surrounding liquid (and the no-slip boundary condition), (ii) viscoelastic behavior with the no-slip boundary condition, and (iii) viscoelastic behavior with the Navier slip condition. Slip lengths and intrinsic quality factors used in the theoretical predictions are obtained by independent fitting to temperature-dependent data for a low glycerol mass fraction of 20%. From [65].

These measurements clearly indicate that slip plays a significant role in nanoscale flows of simple liquids. Moreover, they provide a new means of measuring the slip length, complementing

previous methods and providing the resolution required for the single-nanometer scale slip expected for wetting interfaces. For the water-glycerol mixtures studied, a single slip length of 3.7 ± 0.4 nm reproduces experimental results for all glycerol concentrations.

It is perhaps surprising that slip has a significant and measurable effect, especially for high glycerol concentrations. As described above, slip increases Q for the nanoparticle vibrations when the slip length, b , is comparable to the viscous penetration depth, δ (see Eq. (9)). For high-viscosity liquids, δ is large, and the effect of a few-nanometer slip length would be expected to be negligible. This expectation, however, does not hold for viscoelastic fluids. Elasticity reduces the length scale over which the flow varies relative to a Newtonian flow. In the case of Stokes' second problem, the coefficient, C , in Eq. (10), which specifies the magnitude of this reduction in length scale, becomes [65]

$$C = (1 + \text{De}^2)^{\frac{1}{4}} e^{-i\left(\frac{\pi}{4} + \frac{1}{2}\arctan \text{De}\right)}, \quad (20)$$

which increases with increasing elasticity, i.e., De . This offsets the increase in δ due to increasing viscosity, μ , so that the flow's length scale remains small, and slip can still have an appreciable effect on the nanoparticle vibrations.

Applying the model for extensional vibrations of a slender rod-shaped nanoparticle of radius, R , gives the following sensitivity to slip [65]:

$$S \equiv \left. \frac{d \log Q}{d \Delta} \right|_{\Delta=0} = \left(\frac{R}{\delta} \right)^2 \sqrt{1 + \text{De}^2}, \quad (21)$$

where the parameter $\Delta \equiv (b/\delta)^2$, i.e., the squared ratio of the slip length to the viscous penetration depth, which arises from the analytical shear flow model based on Stokes' second problem. Figure 16 illustrates this sensitivity for water-glycerol mixtures; for high glycerol concentrations, viscoelasticity increases the sensitivity to slip by more than an order of magnitude. This shows that, while slip exerts a negligible effect for highly viscous Newtonian fluids, liquid elasticity enhances this sensitivity to slip and can produce a strong effect in practice.

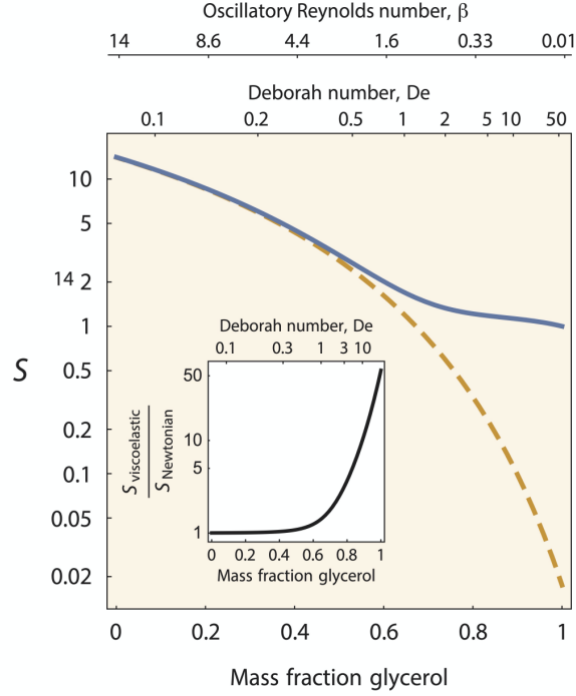


Figure 16. Estimated sensitivity to slip of the quality factor of a cylindrical nanoparticle with a resonance frequency of 20 GHz immersed in water/glycerol mixtures, as a function of the mass fraction of glycerol. The solid blue line accounts for the viscoelastic properties of the liquids and the dashed red line treats the liquids as Newtonian. The inset shows the ratio of the sensitivity to the value it would have if the liquid were Newtonian. From [65].

VII. Conclusions: Towards a New Science of Nanofluidics

Vibrating metal nanoparticles have recently emerged as a new probe of novel fluid mechanics at nanometer length and picosecond time scales, associated with the natural vibrational motion of solid nanoscale objects. In particular, ultrafast time-resolved laser spectroscopy on single nanostructures or monodisperse ensembles of nanoparticles has enabled quantitative measurements of ultrafast, nanoscale fluid-structure interactions. These measurements probe viscoelasticity in simple liquids, slip at the solid-liquid interface, and the synergistic interplay between the two. The vibrational response of metal nanoparticles in water-glycerol mixtures has been shown to be described quantitatively using a linear Maxwell model, with separate shear and

compressional relaxation times. Slip lengths at the single-nanometer scale have been measured, demonstrating the relevance of slip even for wetting interfaces at the nanoscale.

The phenomenological description of nanoscale fluid mechanics afforded by these experiments has broad implications for nanofluidics. Indeed, the viscoelastic response of surrounding liquids is expected to impact the mechanical dynamics of any nanoscale structure undergoing ultrafast motion in a liquid, from nanomotors [118,119] to proteins [120,121]. Emerging technologies also employ motion of nanostructures in liquids; for example, the vibrations of nanoscale objects have recently been developed for mass-based sensing. Adsorption of materials onto a mechanical resonator shifts its resonance frequency, and this shift can be monitored to quantitatively measure the mass that has been deposited. Scaling down the resonator results in a larger fractional frequency shift for a given adsorbed mass, and atomic-scale mass sensitivity has been achieved using nanostructures in vacuum [122,123]. Application of such sensing techniques to biological systems can use the resonators in a liquid environment [124], which in turn will require an understanding of the fluid dynamical effects on the mechanical vibrations of the sensors [125,126]. Viscoelasticity has the potential to at least partially compensate for strong viscous damping expected at nanometer length scales, opening up the possibility of ultrasensitive mass sensing in liquid using high-frequency mechanical vibrations of nanoparticles.

The reported viscoelastic enhancement of slip implies that it will play an especially important role for the ultrafast motion of nanoscale objects in liquid. Nanoscale slip is also known to be important for a range of emerging nanofluidic technologies. For example, the physical mechanisms responsible for enhanced water transport in nanoscale channels [11-13] remain a subject of investigation, but theory and modeling indicate that they are likely related to ultrafast mechanical [127-130] or electronic [131] fluctuations in the walls of the channels. If enhanced nanoscale liquid transport can be understood, it will lead to the rational design of nanoporous membranes for filtration and separation [132,133]; however, a full understanding of the effect of high-frequency wall fluctuations will require a consideration of viscoelasticity in the liquid and its enhancement of interface slip. Beyond these more direct applications, measurements of slip using high-frequency nanoparticle vibrations will provide general mechanistic insight into nanoscale slip at the solid-liquid interface, informing the understanding of slip not only at ultrafast time scales, but also at longer time scales relevant to more conventional applications. The experiments will

thus have potential impact on a wide range of nanofluidic applications, including hydraulic fracturing [134], lab-on-chip systems [135,136], and microscale pumps [137].

The experiments that have been performed so far represent only the beginning of this new experimental approach to nanofluidics. Now that nanoparticles have been shown to provide quantitative information about viscoelasticity and interface slip in simple liquids, a clear next step is to extend the measurements to other liquids with unknown relaxation times and slip lengths, including liquids near phase transitions and liquids with long thermal relaxation times. A key goal is to use smaller particles with faster vibrations [62,63] to access viscoelasticity in water, a liquid of clear technological, biological, and scientific importance. Water is also well known to possess unique physical properties, and studies of its ultrafast nanoscale fluid dynamics may reveal new phenomena particular to this ubiquitous liquid.

In fact, preliminary measurements have already indicated the presence of a nonlinear mechanical response in water. Four-wave mixing measurements of small vibrating gold nanoparticles in water showed a rapid increase in signal above a threshold laser power [138]. Molecular-dynamics (MD) simulations suggest that this threshold is due to a cavitation effect, where a rarified region of liquid is formed around the nanoparticle as it contracts because the motion of the surrounding liquid molecules is slower than the motion of the nanoparticle surface [139]. This experiment illustrates the opportunity that remains to discover new nanofluidic phenomena through the measurement of nanoparticle vibrations.

MD modeling also illustrates the value of combining continuum and microscopic descriptions of liquid response. Use of MD to provide insight into the molecular relaxation modes responsible for the measured relaxation times in simple liquids may even allow for a microscopic derivation of these relaxation times; and similarly for slip lengths. In this way, the combination of modeling and experiment can help to address the central challenge of molecular liquid dynamics: how to describe bulk liquid response in terms of the interactions among the molecules that make up the liquid [140].

Acknowledgments

M.P. and B.U. acknowledge funding from the U.S. National Science Foundation under grant DMR-1554895. J.E.S. acknowledges support from the Australian Research Council Grants Scheme and the Australian Research Council Centre of Excellence in Exciton Science (CE170100026).

References

- [1] Batchelor G K 2000 *An Introduction to Fluid Dynamics* (Cambridge: Cambridge University Press)
- [2] Landau L D and Lifshitz E M 1959 *Fluid Mechanics* (Oxford: Pergamon)
- [3] Schowalter W R 1978 *Mechanics of Non-Newtonian Fluids* (Oxford: Pergamon)
- [4] Maxwell J C 1867 IV. On the dynamical theory of gases *Phil. Trans. Roy. Soc.* **157** 49
- [5] Chakraborty D and Sader J E 2015 Constitutive models for linear compressible viscoelastic flows of simple liquids at nanometer length scales *Phys. Fluids* **27** 052002
- [6] Flory P and Volkenstein M 1969 *Statistical Mechanics of Chain Molecules* (New York: Interscience Publishers)
- [7] Yong W A 2014 Newtonian limit of Maxwell fluid flows *Arch. Ration. Mech. Anal.* **214** 913
- [8] Goldstein S 1969 Fluid mechanics in the first half of this century *Ann. Rev. Fluid Mech.* **1** 1
- [9] Neto C, Evans D R, Bonaccorso E, Butt H-J and Craig V S 2005 Boundary slip in Newtonian liquids: a review of experimental studies *Rep. Prog. Phys.* **68** 2859
- [10] Koplik J and Banavar J R Corner flow in the sliding plate problem 1995 *Phys. Fluids* **7** 3118

- [11] Majumder M, Chopra N, Andrews R and Hinds B J 2005 Enhanced flow in carbon nanotubes *Nature* **438** 44
- [12] Holt J K, Park H G, Wang Y, Stadermann M, Artykhin A B, Grigoropoulos C P, Noy A and Bakajin O 2006 Fast mass transport through sub-2-nanometer carbon nanotubes *Science* **312** 1034
- [13] Seechi E, Marbach S, Niguès A, Stein D, Siria A and Bocquet L 2016 Massive radius-dependent flow slippage in carbon nanotubes *Nature* **537** 210
- [14] Maxwell J C 1879 VII. On stresses in rarified gases arising from inequalities of temperature *Phil. Trans. R. Soc.* **170** 231
- [15] Lauge E, Brenner M and Stone H 2007 Microfluidics: The no-slip boundary condition. In: Tropea C, Yarin A L, and Foss J F (eds) *Springer Handbook of Experimental Fluid Mechanics* (Berlin: Springer)
- [16] Cao B Y, Sun J, Chen M and Guo Z-Y 2009 Molecular momentum transport at fluid-solid interfaces in MEMS/NEMS: A review *Int. J. Mol. Sci.* **10** 4638
- [17] Bocquet L and Charlaix E 2010 Nanofluidics, from bulk to interfaces *Chem. Soc. Rev.* **39** 1073
- [18] Shu J-J, Teo J B M and Chan W K 2017 Fluid velocity slip and temperature jump at a solid surface *Appl. Mech. Rev.* **69** 020801
- [19] Thompson P A and Troian S M 1997 A general boundary condition for liquid flow at solid surfaces *Nature* **389** 360
- [20] Barrat J L and Bocquet L 1999 Large slip effect at a nonwetting fluid solid interface *Phys. Rev. Lett.* **82** 4671
- [21] Huang D M, Sendner C, Horinek D, Netz R R and Bocquet, L 2008 Water slippage versus contact angle: A quasiuniversal relationship *Phys. Rev. Lett.* **101** 226101

- [22] Voronov R S, Papavassiliou D V and Lee L L 2008 Review of fluid slip over superhydrophobic surfaces and its dependence on the contact angle *Ind. Eng. Chem. Res.* **47** 2455
- [23] Richardson S 1973 On the no-slip boundary condition *J. Fluid Mech.* **59** 707
- [24] Migler J, Hervet H and Leger L 1993 Slip transition of a polymer melt under shear stress *Phys. Rev. Lett.* **70** 287
- [25] Denn M M 2001 Extrusion instabilities and wall slip *Annu. Rev. Fluid Mech.* **33** 265
- [26] Cross B, Barraud C, Picard C, Léger L, Restagno L and Charlaix É 2018 Wall slip of complex fluids: Interfacial friction versus slip length *Phys. Rev. Fluids* **3** 062001
- [27] Léger L, Hervet L, Massey G and Durliat E 1997 Wall slip in polymer melts *J. Phys.: Cond. Matt.* **9** 7719
- [28] Barnes H A 1995 A review of the slip (wall depletion) of polymer solutions, emulsions and particle suspensions in viscometers: its cause, character, and cure *J. Non-Newtonian Fluid Mech.* **56**, 221
- [29] Comez L, Masciovecchio C, Monaco G and Fioretto D 2012 Progress in liquid and glass physics by Brillouin scattering spectroscopy *J. Phys. C: Solid State Phys.* **63** 1
- [30] Teixeira J, Bellissent-Funel M-C, Chen S H and Dianous A J 1985 Experimental determination of the nature of diffusive motions of water molecules at low temperatures *Phys. Rev. A* **31** 1913
- [31] Amman-Winkler K, Bellissent-Funel M-C, Bove L E, Loerting T, Nilsson A, Paciaroni A, Schlesinger D and Skinner L, X-ray and neutron scattering of water *Chem. Rev.* **116** 7570
- [32] Monaco G, Cunsolo G, Ruocco G and Sette F 1999 Viscoelastic behavior of water in the terahertz-frequency range: An inelastic x-ray scattering study *Phys. Rev. E* **60** 5505
- [33] Cunsolo A 2017 The terahertz dynamics of simplest fluids probed by inelastic x-ray scattering *Int. Rev. Phys. Chem.* **36** 433

- [34] Piccirelli R and Litovitz T A 1957 Ultrasonic shear and compressional relaxation in liquid glycerol *J. Acoust. Soc. Am.* **29** 1009
- [35] Slie W, Donfor A R Jr. and Litovitz T A 1966 Ultrasonic shear and longitudinal measurements in aqueous glycerol *J. Chem. Phys.* **44** 3712
- [36] Pezeril T, Klieber C, Andrieu S and Nelson K A 2009 Optical generation of gigahertz-frequency shear acoustic waves in liquid glycerol *Phys. Rev. Lett.* **102** 107402
- [37] Klieber C, Pezeril T, Andrieu S and Nelson K A 2012 Optical generation and detection of gigahertz-frequency longitudinal and shear acoustic waves in liquids: Theory and experiment *J. Appl. Phys.* **112** 013502
- [38] Klieber C, Hecksher T, Pezeril T, Torchinsky D H, Dyre J C and Nelson K A 2013 Mechanical spectra of glass-forming liquids. II. Gigahertz-frequency longitudinal and shear acoustic dynamics in glycerol and DC704 studied by time-domain Brillouin scattering *J. Chem. Phys.* **138** 12A544
- [39] Klieber C, Gusev V E, Pezeril T and Nelson K A 2015 Nonlinear acoustics at GHz frequencies in a viscoelastic fragile glass former *Phys. Rev. Lett.* **114** 065701
- [40] Baudry J, Charlaix E, Tonck A and Mazuyer D 2001 Experimental evidence for a large slip effect at a nonwetting fluid-solid interface *Langmuir* **17** 5232
- [41] Bonaccursa E, Butt H-J and Craig V S 2003 Surface roughness and hydrodynamic boundary slip of a Newtonian fluid in a completely wetting system *Phys. Rev. Lett.* **90** 144501
- [42] Zhu Y and Granick S 2002 Limits of the hydrodynamic no-slip boundary condition *Phys. Rev. Lett.* **88** 106102
- [43] Campbell S E, Luengo G, Srandov V I, Wudl F and Israelachvili J N 1996 Very low viscosity at the solid-liquid interface induced by adsorbed C₆₀ monolayers *Nature* **382** 520
- [44] Bonaccurso E, Kappl M and Butt H-J 2002 Hydrodynamic force measurements: Boundary slip of water on hydrophilic surfaces and electrokinetic effects *Phys. Rev. Lett.* **88** 076103

- [45] Cho J-H J, Law B M and Rieutord F 2004 Dipole-dependent slip of Newtonian liquids at smooth hydrophobic surfaces *Phys. Rev. Lett.* **92** 166102
- [46] Vinogradova O I and Yakubov G E 2003 Dynamic effects on force measurements. 2. Lubrication and the atomic force microscope *Langmuir* **19** 1227
- [47] Henry C L, Neto C, Evans D R, Biggs S and Craig V S J 2004 The effect of surfactant adsorption on liquid boundary slippage *Physica A* **339** 60
- [48] Zhu L, Attard P and Neto C 2012 Reliable measurements of interfacial slip by colloid probe force microscopy. II. Hydrodynamic force measurements *Langmuir* **28** 7768
- [49] Vinogradova O I 1995 Drainage of a thin liquid film confined between hydrophobic surfaces *Langmuir* **11** 2213
- [50] Bureau L 2010 Nonlinear rheology of a nanoconfined simple fluid *Phys. Rev. Lett.* **104** 218302
- [51] Labuda A, Kobayashi K, Suzuki K, Yamada H and Grütter P 2013 Monotonic damping in nanoscopic hydration experiments *Phys. Rev. Lett.* **110** 066102
- [52] Whitby M and Quirke N 2007 Fluid flow in carbon nanotubes and nanopipes *Nat. Nanotechnol.* **2** 87
- [53] Ou J and Rothstein J P Direct velocity measurements of the flow past drag-reducing ultrahydrophobic surfaces *Phys. Fluids* **17** 103606
- [54] Huang P, Guasto J S and Breuer K S 2006 Direct measurement of slip velocities using three-dimensional total internal reflection velocimetry *J. Fluid Mech.* **566** 447
- [55] Lauga E and Squires T M 2005 Brownian motion near a partial-slip boundary: A local probe of the no-slip condition *Phys. Fluids* **17** 103102
- [56] Li Z, D'eraimo L, Monti F, Vayssade A L, Chollet B, Bresson B, Tran Y, Cloitre M and Tabeling P 2014 Slip length measurements using μ PIV and TIRF-based velocimetry *Isr. J. Chem.* **54** 1589

- [57] Guasto J S, Hyang P and Breuer K S 2006 Statistical particle tracking velocimetry using molecular and quantum dot tracer particles *Exp. Fluids* **41** 869
- [58] Jin S, Huang P, Park J, Yoo J and Breuer K 2004 Near-surface velocimetry using evanescent wave illumination *Exp. Fluids* **37** 825
- [59] Collis J F, Olcum S, Chakraborti D, Manails S R and Sader J E 2021 Measurement of Navier slip on individual nanoparticles in liquid *Nano Lett.* **21** 4959
- [60] Hartland G V 2011 Optical studies of dynamics in noble metal nanostructures *Chem. Rev.* **111** 3858
- [61] Yu K, Jiang Y, Wright C, and Hartland GV 2022 Energy dissipation for nanometer sized acoustic oscillators *J. Phys. Chem. C* DOI: 10.1021/acs.jpcc.1c10073
- [62] Juvé V, Maioli P, Pellarin M, Broyer M, Del Fatti N and Vallée F 2010 Probing elasticity at the nanoscale: Terahertz acoustic vibration of small metal nanoparticles *Nano Lett.* **10** 1853
- [63] Maioli P, Stoll T, Saucedo H E, Valencia I, Demessence A, Bertorelle F, Crut A, Vallée F, Garzón I L, Cerulla G and Del Fatti N 2018 Mechanical vibrations of atomically defined metal clusters: From nano- to molecular-sized oscillators *Nano Lett.* **18** 6842
- [64] Pelton M, Chakraborty D, Malachosky E, Guyot-Sionnest P and Sader J E 2013 *Phys. Rev. Lett.* **111** 224502
- [65] Chakraborty D, Uthe B, Malachosky E W, Pelton M and Sader J E 2021 Viscoelasticity enhances nanometer-scale slip in gigahertz-frequency liquid flows *J. Phys. Chem. Lett.* **12** 3449
- [66] Maier S A 2007 *Plasmonics: Fundamentals and Applications* (New York: Springer)
- [67] Pelton M and Bryant G W 2013 *Introduction to Metal-Nanoparticle Plasmonics* (Hoboken: Wiley)
- [68] Bohren C F and Huffman D R 2008 *Absorption and Scattering of Light by Small Particles* (New York: John Wiley & Sons)

- [69] Weitz D A, Gramila T J, Genack A Z and Gersten J I 1980 Anomalous low-frequency Raman scattering from rough metal surfaces and the origin of surface-enhanced Raman scattering *Phys. Rev. Lett.* **45** 355
- [70] Gersten J I, Weitz D A, Gramila T J and Genack A Z 1980 Inelastic Mie scattering from rough metal surfaces: Theory and experiment *Phys. Rev. B* **22** 4562
- [71] Mariotto G, Montagna M, Viliani G, Duval E, Lefrant S, Rzepka E and Mai C 1988 Low-energy Raman scattering from silver particles in alkali halides *Europhys. Lett.* **6** 239
- [72] Fujii M, Nagareda T, Hayashi S and Yamamoto K 1991 Low-frequency Raman scattering from small silver particles embedded in SiO₂ thin films *Phys. Rev.* **44** 6243
- [73] Bachelier G and Mlayah A 2004 Surface plasmon mediated Raman scattering in metal nanoparticles *Phys. Rev. B* **69** 205408
- [74] Portales G, Saviot L, Duval M, Fujii M, Hayashi S, Del Fatti N and Vallée F 2001 Resonant Raman scattering by breathing modes of metal nanoparticles *J. Chem. Phys.* **115** 3444
- [75] Courty A, Lisieki I and Pileni M P 2002 Vibration of self-organized silver nanocrystals *J. Chem. Phys.* **116** 8074
- [76] Large N, Saviot L, Marueritat J, Gonzalo J, Afonzo C N, Arbouet A, Langot P, Mlayah A and Aizpurua J 2009 Acousto-plasmonic hot spots in metallic nano-objects *Nano Lett.* **9** 3732
- [77] Girard A, Gehan H, Crut A, Mermet A, Saviot L and Margueritat J 2016 Mechanical coupling in gold nanoparticles supermolecules revealed by plasmon-enhanced ultralow frequency Raman spectroscopy *Nano Lett.* **16** 3843
- [78] Girard A, Gehan H, Mermet A, Bonnet C, Lermé J, Berthelot A, Cottancin E, Crut A, and Margueritat J 2018 Acoustic mode hybridization in a single dimer of gold nanoparticles *Nano Lett.* **18** 3800
- [79] Xiang D and Gordon R 2016 Nanoparticle acoustic resonance enhanced nearly degenerate four-wave mixing *ACS Photon.* **3** 1421

- [80] Wu J, Xiang D and Gordon R 2016 Characterizing gold nanorods in aqueous solution by vibrations probed with four-wave mixing *Opt. Express* **24** 12458
- [81] Xiang D and Gordon R 2016 Nanoparticle acoustic resonance enhanced nearly degenerate four-wave mixing *ACS Photon.* **3** 1421
- [82] Wu J, Xiang G, Hajisalen G, Lin F-C, Huang J-S, Kuo C-H and Gordon R 2016 Probing the acoustic vibrations of complex-shaped metal nanoparticles with four-wave mixing *Opt. Express* **24** 23747
- [82] Nisoli M, De Silvestri S, Cavalleri A, Malvezzi A, Stella A, Lanzani G, Cheyssac P and Kofman R 1997 Coherent acoustic oscillations in metallic nanoparticles generated with femtosecond optical pulses *Phys. Rev. B* **55** R13424
- [83] Hodak J. G, Martini I and Hartland G V 1998 Observation of acoustic quantum beats in nanometer sized Au particles *J. Chem. Phys.* **108** 9210
- [84] Hartland G V 2006 Coherent excitation of vibrational modes in metallic nanoparticles *Annu. Rev. Phys. Chem.* **57** 403
- [85] Tchebotareva A L, Ruijgrok P V, Zijlstra P and Orrit M 2010 Probing the acoustic vibrations of single metal nanoparticles by ultrashort laser pulses *Laser Photon. Rev.* **4** 581
- [86] Crut A, Mailoi P, Del Fatti N and Vallée F 2015 Acoustic vibrations of metal nano-objects: Time-domain investigations *Phys. Rep.* **549** 1
- [87] Ahmadi T S, Logunov S L and El-Sayed M A 1996 Picosecond dynamics of colloidal gold nanoparticles *J. Phys. Chem.* **100** 8053
- [88] Hodak J H, Martini I and Hartland G V 1998 Spectroscopy and dynamics of nanometer-sized noble metal particles *J. Phys. Chem. B* **102** 6958
- [89] Hodak J H, Henglein A and Hartland G V 1999 Size dependent properties of Au particles: Coherent excitation and dephasing of acoustic vibrational modes *J. Chem. Phys.* **111** 8613

- [90] Petrova A, Lin C-H, de Liejer, S, Hu M, McLellan J M, Siekkinen A R, Wiley B J, Marquez M, Xia Y, Sader J E and Hartland G V. 2007 Time-resolved spectroscopy of silver nanocubes: Observation and assignment of coherently excited vibrational modes, *J. Chem. Phys.* **126** 294709
- [91] Ahmed A, Pelton M and Guest J R 2017 Understanding how acoustic vibrations modulate the optical response of plasmonic metal nanoparticles *ACS Nano* **11** 9360
- [92] Seferyan H Ye, Zadoyan R, Wark A W, Corn R M and Apkarian V A 2007 Diagnostics of spectrally resolved transient absorption: Surface plasmon resonance of metal nanoparticles *J. Phys. Chem. C* **111** 18525
- [93] Hartland G V 2010 Ultrafast studies of single semiconductor and metal nanostructures through transient absorption microscopy *Chem. Sci.* **1** 303
- [94] Beane G, Devkota T, Brown B S and Hartland G V 2019 Ultrafast measurements of the dynamics of single nanostructures: a review *Rep. Prog. Phys.* **62** 016401
- [95] van Dijk M A, Lippitz M, Stolwijk D and Orrit M 2007 A common-path interferometer for time-resolved and shot-noise-limited detection of single nanoparticles *Opt. Express* **15** 2273
- [96] Staleva H and Hartland G V 2008 Vibrational dynamics of silver nanocubes and nanowires studied by single-particle transient absorption spectroscopy *Adv. Funct. Mater.* **18** 3809
- [97] Zijlstra P, Tchegbotareva A L, Chon J W M, Gu M and Orrit M 2008 Acoustic oscillations and elastic moduli of single gold nanorods **8** 3493
- [98] Marty R, Arbouet A, Girard C, Mlayah A, Paillard V, Lin V K, Teo S L and Tripathy S 2011 Damping of the acoustic vibrations of individual gold nanoparticles *Nano Lett.* **11** 3301
- [99] Voisin C, Christofilos D, Del Fatti N and Vallée F 2002 Environmental effect on the acoustic vibration of metal nanoparticles *Physica B* **316** 89
- [100] Yu K, Zijlstra P, Sader J E, Xu Q-H and Orrit M 2013 Damping of acoustic vibrations of immobilized single gold nanorods in different environments *Nano Lett.* **13** 2710

- [101] Ruijgrok P V, Zijlstra P, Tchebotareva A L and Orrit M 2012 Damping of acoustic vibrations of single gold nanoparticles optically trapped in water *Nano Lett.* **12** 1063
- [102] Major T A, Crut A, Gao B, Lo S S, Del Fatti N, Vallée F and Hartland G V 2013 Damping of the acoustic vibrations of suspended gold nanowire in air and water environments *Phys. Chem. Chem. Phys.* **15** 4169
- [103] Hartland G V 2002 Coherent vibrational motion in metal particles: Determination of the vibrational amplitude and excitation mechanism *J. Chem. Phys.* **116** 8048
- [104] Pelton M, Sader J E, Burgin J, Liu M, Guyot-Sionnest P and Gosztola D 2009 Damping of acoustic vibrations in gold nanoparticles *Nat. Nanotechnol.* **4** 492
- [105] Pelton M, Wang Y, Gosztola D and Sader J E 2011 Mechanical damping of longitudinal acoustic oscillations of metal nanoparticles in solution *J. Phys. Chem. C* **115** 23732
- [106] Liu M and Guyot-Sionnest P 2005 Mechanism of silver(I)-assisted growth of gold nanorods and bipyramids *J. Phys. Chem. B* **109** 22192
- [107] Chakraborty D, van Leeuwen E, Pelton M and Sader J E 2013 Vibration of nanoparticles in viscous fluids *J. Phys. Chem. C* **117** 8536
- [108] Yu K, Major T A, Chakraborty D, Devadas M S, Sader J E and Hartland G V 2015 Compressible viscoelastic liquid effects generated by the breathing modes of isolated metal nanowires *Nano Lett.* **15** 3964
- [109] Devkota T, Chakraborty D, Yu K, Beane G, Sader J E and Hartland G V 2018 On the measurement of relaxation times of acoustic vibrations in metal nanowires *Phys. Chem. Chem. Phys.* **20** 17687
- [110] Chakraborty D, Hartland G V, Pelton M and Sader J E 2017 When can the elastic properties of simple liquids be probed using high-frequency nanoparticle vibrations? *J. Phys. Chem. C* **122** 13347

- [111] Major T A, Devadas M S, Lo S S and Hartland G V 2013 Optical and dynamical properties of chemically synthesized gold nanoplates *J. Phys. Chem. C* **117** 1447
- [112] Devkota T, Yu K and Hartland G V 2019 Mass loading effects in the acoustic vibrations of gold nanoplates *Nanoscale* **11** 16208
- [113] Yu K, Devkota T, Beane G, Wang G P and Hartland G V 2017 Brillouin oscillations from single Au nanoplate opto-acoustic transducers *ACS Nano* **11** 8064
- [114] Yu K, Yang Y, Wang J, Hartland G V and Wang G P 2021 Nanoparticle-fluid interactions at ultrahigh acoustic vibration frequencies studied by femtosecond time-resolved microscopy *ACS Nano* **15** 1833
- [115] Lee J-Y, Schade N B, Fan J A, Bae D R, Mariscal M M, Lee G, Capasso F, Sacanna S, Manoharan V N and Yi G-R 2013 UltrasMOOTH, highly spherical monocrystalline gold particles for precision plasmonics *ACS Nano* **7** 11064
- [116] Saunders A E, Garcia D A and Oldenburg, S. J. 2018 Ultra uniform colloidal particles as nanoscale reference materials. *TechConnect Briefs: Adv. Mater.* **1** 1
- [117] Uthe B, Collis J F, Madadi M, Sader J E and Pelton M 2021 Highly spherical nanoparticles probe gigahertz viscoelastic flows of simple liquids without the no-slip condition *J. Phys. Chem. Lett.* **12** 4440
- [118] Wang H and Pumera M 2015 Fabrication of micro/nanoscale motors *Chem. Rev.* **115** 8704
- [119] Peng F, Tu Y and Wilson D A 2017 Micro/nanomotors towards *in vivo* application: cell, tissue and biofluid *Chem. Soc. Rev.* **57** 5289
- [120] Bao G and Suresh S 2003 Cell and molecular mechanics of biological materials *Nat. Mater.* **2** 715
- [121] Khodadadi S and Sokolov A P Protein dynamics: from rattling in a cage to structural relaxation *Soft Matter* **11** 4984

- [122] Yang Y, Callegari C, Feng X L, Ekinici K L and Roukes M 2006 Zeptogram-scale nanomechanical mass sensing *Nano Lett.* **6** 583
- [123] Arlett J L, Myers E B and Roukes M L 2011 Comparative advantages of mechanical biosensors *Nat. Nanotechnol.* **6** 203
- [124] Johnson B N and Mutharasan R 2011 Biosensing using dynamic-mode cantilever sensors: a review *Biosens. Bioelectron.* **32** 1
- [125] Basak S, Raman A and Garimella S V 2006 Hydrodynamic loading of microcantilevers vibrating in viscous fluids *J. Appl. Phys.* **99** 114906
- [126] Sawano S, Arie T and Akita S 2010 Carbon nanotube resonator in liquid *Nano Lett.* **10** 3395
- [127] Ma M, Grey F, Shen L, Urbakh M, Wu S, Liu J Z, Liu Y and Zheng Q 2015 Water transport inside carbon nanotubes mediated by phonon-induced oscillating friction *Nat. Nanotech.* **10** 692
- [127] Cruz-Chú E R, Papadopoulou E, Walther J H, Popadić A, Li G, Praprotnik M and Koumoutsakos P 2017 On phonons and water flow enhancement in carbon nanotubes *Nat. Nanotech.* **12**,1106
- [129] Cao W, Wang J and Ma M 2019 Water diffusion in wiggling graphene membranes *J. Phys. Chem. Lett.* **10** 7251
- [130] Marbach S, Dean D S and Bocquet L 2018 Transport and dispersion across wiggling nanopores *Nat. Phys.* **14** 1108
- [131] Kavokine N, Bocquet M-L, and Bocquet L 2022 Fluctuation-induced quantum friction in nanoscale water flows *Nature* **602** 84
- [132] Nair R, Wu H, Jayaram P, Grigorieva I and Geim A 2012 Unimpeded permeation of water through helium-leak-tight graphene-based membranes *Science* **335** 442

- [133] Wang L, Boutilier M S, Kidambi P R, Jang D, Hadjiconstantinou N G and Karnik R 2017 Fundamental transport mechanisms, fabrication and potential applications of nanoporous atomically thin membranes *Nat. Nanotechnol.* **12** 509
- [134] Javadpour F, McClure M and Naraghi M 2015 Slip-corrected liquid permeability and its effect on hydraulic fracturing and fluid loss in shale *Fuel* **160** 549
- [135] Stone H A, Stroock A D and Ajdari A 2004 Engineering flows in small devices: Microfluidics towards lab-on-a-chip *Annu. Rev. Fluid Mech.* **36** 381
- [136] Tabeling P 2009 A brief introduction to slippage, droplets and mixing in microfluidic systems *Lab Chip* **9** 2428
- [137] Matthews M T and Hill J M 2008 Lubrication analysis of the viscous micro/nano pump with slip *Microfluid. Nanofluid.* **4** 439
- [138] Xiang D, Wu J, Rottler J and Gordon R 2016 Threshold for terahertz resonance of nanoparticles in water *Nano Lett.* **16** 3638
- [139] Hsueh C-C, Gordon R and Rottler J 2018 Dewetting during terahertz vibrations of nanoparticles *Nano Lett.* **18** 773
- [140] Boon J P and Yip S 1980 *Molecular Hydrodynamics* (New York: McGraw-Hill)